综述论文

DOI：10.11949/0438-1157.20251319

基于树枝状结构的核壳型纳米反应器研究进展

王亚斌[1]，黄亮珠[1]，赵文廷[2]，丁秀萍[3]

（[1]延安大学化学与化工学院，陕西 延安 716000；[2]内蒙古科学技术研究院矿产资源利用与冶金研究所，内蒙古 呼和浩特 010070；[3]中国科学院青海盐湖研究所中国科学院盐湖资源综合高效利用重点实验室，青海 西宁 810008）

摘要： 核壳型纳米反应器由内层核芯材料和另一种外壳材料复合而成。当树枝状介孔材料作为其中之一时，基于树枝状结构的核壳型纳米反应器应运而生，包括磁性核@树枝状壳、非磁性核@树枝状壳、树枝状核@介孔壳等多种类型。这些复合体兼备构成材料的物理化学特性，在重金属吸附、催化合成、分子检测、生物酶固定、药物递送等领域具有广泛的应用前景和优势。截至目前，还未出现介绍该类纳米材料的综述文章。因此，本文主要归纳分析树枝状核壳结构纳米反应器的分类，每种类型的结构特征、制备方法及应用领域，分析展望该学科今后的研究重点及发展前景。期望本综述能够给予材料和化学科学家一些参考，加速树枝状核壳结构纳米反应器的蓬勃发展。

关键词： 化学反应器；复合材料；纳米粒子；纳米结构；二氧化硅

中图分类号： TB33　　**文献标志码：** AA

文章编号： 0438-1157（XXXX）XX-0001-24

Research progress in core-shell nanoreactors on the basis of dendritic architectures

WANG Yabin[1], HUANG Liangzhu[1], ZHAO Wenting[2], DING Xiuping[3]

([1]*College of Chemistry and Chemical Engineering, Yan'an University, Yan'an* 716000, *Shaanxi, China*; [2]*Institute of Mineral Resources Utilization and Metallurgy, Inner Mongolia Academy of Science and Technology, Hohhot* 010070, *Inner Mongolia, China*; [3]*Key Laboratory of Comprehensive and Highly Efficient Utilization of Salt Lake Resources, Qinghai Institute of Salt Lakes, Chinese Academy of Sciences, Xining* 81008, *Qinghai, China*)

Abstract: Core-shell nanoreactors are composed of an inner core material and an outer shell one. When the dendritic mesoporous material serves as one component, dendritic-based core-shell nanoreactors can be developed, covering magnetic core@dendritic shell, non-magnetic core@dendritic shell, dendritic core@mesoporous shell, and so on. These composites combine physicochemical properties of the constituent entities and possess broad application prospects and advantages in multiple fields, like chemical adsorption of heavy metal, catalytic synthesis, molecular detection, enzyme immobilization, drug delivery, and so forth. Up to date, no review has been officially published with respect to this type of nanomaterial. This paper not only systematically categorizes dendritic core-shell nanoreactors and analyzes their structural characteristics, preparation methods, as well as application domains, but also outlines future research priorities and development prospects in this field. It is expected that this review

收稿日期： 2025-11-25　　**修回日期：** 2025-12-26

通信作者： 赵文廷(1995—)，男，博士，副研究员，zhaowt@imast.ac.cn

第一作者： 王亚斌(1984—)，男，博士，副教授，ybw@yau.edu.cn

基金项目： 国家重点研发计划项目(2024YFC3909300)；国家自然科学基金(52363029)；内蒙古科学技术研究院产业技术创新项目(2024RCYJ05002)

引用本文： 王亚斌, 黄亮珠, 赵文廷, 丁秀萍. 基于树枝状结构的核壳型纳米反应器研究进展[J]. 化工学报, DOI: 10.11949/0438-1157.20251319

Citation: WANG Yabin, HUANG Liangzhu, ZHAO Wenting, DING Xiuping. Research progress in core-shell nanoreactors on the basis of dendritic architectures[J]. CIESC Journal, DOI: 10.11949/0438-1157.20251319

could serve as a reference for material and chemical scientists, accelerating the vigorous development of dendritic-based core-shell nanoreactors.

Keywords: chemical reactors; composites; nanoparticles; nanostructure; silica

引 言

正文核壳型纳米反应器由内层材料(核芯)和外层另一种材料(壳层)复合而成[1-2]。自20世纪初至今,已有大量研究集中在该类粒子的设计构筑与先进应用。通过合理配置内外层材料,中心核与壳层融合一体,从而展现出全新的物理化学特性,从而实现定向应用。核壳型纳米反应器的性能是单一组分材料无法实现和获得的。例如在药物递送领域,磁性中心核搭配多孔二氧化硅外壳备受青睐,因其兼备了磁响应和装载功能。当然,核壳型纳米反应器存在局限性,如在批量合成过程中丧失固有物理化学特性、均匀性不佳、商业化供应受限等。迄今为止,已有大量高质量综述总结了核壳型材料的分类、性质、合成机制、表征及应用等[3-4]。Yue等人系统总结了借助界面共组装技术对介孔二氧化硅磁性核壳材料进行合理设计与精准调控,涉及壳层孔道结构、壳表面形貌、核壳空间排布等,并展示了该类材料在吸附、催化及生物递送等领域的应用潜力[5]。Shafiee等人则重点综述了构建核壳、蛋黄-蛋壳及多层核壳等纳米结构的策略,分析了界面调控能带结构与电荷传输路径的机制,从而为合理设计高效光催化剂提供思路[6]。截至目前,没有以树枝状结构为核芯或壳层来构筑复合纳米反应器的文献报道。本综述归纳总结以树枝状结构为基础的核壳型纳米反应器最新研究进展,包括其分类、设计合成策略、先进及潜在应用等。

树枝状(dendritic)结构字面意思为树木分支状(图1a_1),立体组装后呈球形,其截面近似于圆(图1a_2)。高分子化学领域的树枝状大分子结构乃其引申意义(图1a_3)[7-8]。2010年,阿卜杜拉国王科技大学催化研究中心(KAUST Catalysis Center)Polshettiwar等采用微乳液法首次合成了具有类似树枝状大分子特殊形貌的二氧化硅介孔纳米球(KCC-1,如图1b所示),拉开了“树枝状”二氧化硅无机材料领域的研究序幕[9]。经过近15年的发展,树枝状介孔纳米粒子(dendritic mesoporous nanoparticles, DMNs)取得了长足进步。DMNs特异三维中心辐射状孔道和多级孔结构使其拥有较高比表面积、较大孔体积、较易孔渗透性和颗粒内表面更易接触性等优点。客体物质能够沿着中心辐射状孔道进行负载和输送,甚至与化学改性所得内部活性位点发生反应。因此,DMNs被证明是一类极具前景的载体平台,可以用来设计构筑为催化剂、吸附剂、递送系统等纳米反应器[10-13]。截至目前,科研工作者不仅开发出不同材质DMNs,如二氧化硅基(dendritic mesoporous silica nanoparticles, DMSNs)[14]、碳材料基(dendritic mesoporous carbon nanoparticles, DMCNs)[15]、有机硅基(dendritic mesoporous organosilica nanoparticles, DMONs)[16]等;而且构筑了兼具其他特殊形貌DMNs,如球形磁性核壳结构(magnetic core-shell)[17]、羽毛球状(shuttlecock-shaped)[18]、双面神状(Janus)[19]等。最为重要的是,通过对原料或工艺的调整,能够合成具有不同粒径、壁厚或孔径的DMNs,进而实现特殊应用需求[14,20]。如图1c为本团队制备具有相近粒径但孔径分布差异巨大的系列DMSNs,其能负载不同尺寸大小客体物质。大量研究表明:DMSNs基材料性能优于传统二氧化硅基材料(如MCM-41和SBA-15),能够成为理想升级替代品[10-13]。

随着对树枝状纳米粒子的研究愈发深入,基于DMNs的核壳型纳米反应器开始崭露头角。按照有无磁性材料参与组成,可分为磁性和非磁性两大类。其中,磁性(magnetic)核壳型纳米反应器可具体为单一材料核壳型、多样材料核壳型以及蛋黄-蛋壳型,分别简记为M@DMNs(图1d_1)、M@barrier@DMNs(图1d_2)和M@void@DMNs(图1d_3)。而非磁性(non-magnetic)核壳型纳米反应器可具体为DMNs当作壳层紧贴中心核、DMNs当作壳层与中心核有间隙或DMNs当作中心核的复合结构,分别简记为NM@DMNs(图1d_4)、NM@void@DMNs(图1d_5)和DMNs@NM(图1d_6)。上述6种核壳型纳米反应器是构成吸附剂、催化剂、递送系统等反应平台的基本结构。在深入理解此类纳米材料时,值得注意三点。第一,DMNs绝大多数为球状,因此也被定义为“dendritic mesoporous nanospheres”,即“树枝状介孔纳米球”。第二,DMNs中最容易制备和研究最为广泛的为二氧化硅基

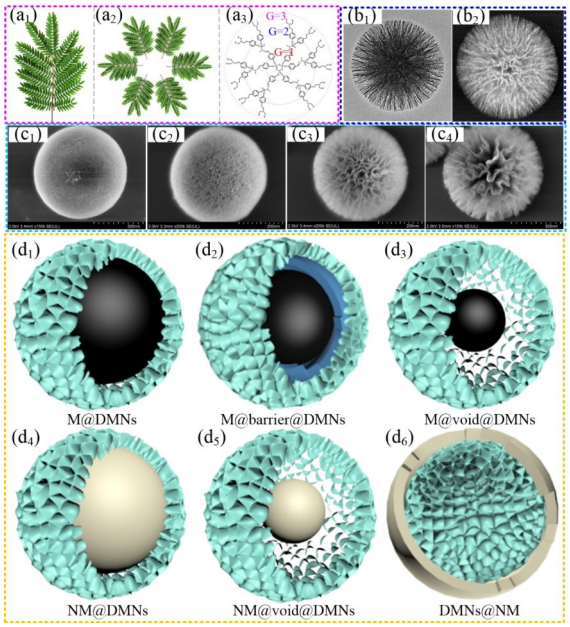

图1 (a) 自然界具有“树枝状”结构的树木分支实物图(a_1)；(a_2) 树木分支实物的环状结构；(a_3) 带有功能基团的树枝状大分子示意图；(b) 本文作者课题组制得DMSNs的透射电镜(b_1)和次级电子(SE，b_2)图像；(c) 本文作者课题组制得具有小孔(c_1)；中孔(c_2)；大孔(c_3)和极大孔(c_4)的DMSNs；(d)树枝状磁性单一材料核壳型M@DMNs(d_1)；磁性多样材料核壳型M@barrier@DMNs(d_2)；磁性蛋黄-蛋壳型M@void@DMNs(d_3)；非磁性核壳型NM@DMNs(d_4)；非磁性蛋黄-蛋壳型NM@void@DMNs(d_5)和非磁性核壳型DMNs@NM(d_6)纳米粒子结构模型

Fig.1 (a) A photograph of a tree branch in nature with “dendritic” architecture (a_1); the loop of the above tree branches (a_2); and a branched organic macromolecule with functional groups (a_3); (b) TEM (b_1) and secondary electron (SE, b_2) images of a single DMSNs synthesized by our team; (c) DMSNs with small (c_1); medium (c_2); large (c_3); and extra-large (c_4) pores in our laboratory; (d) Structural models of simple dendritic magnetic core-shell M@DMNs (d_1); composite dendritic magnetic core-shell M@barrier@DMNs (d_2); dendritic magnetic yolk-shell M@void@DMNs (d_3); as well as dendritic non-magnetic core-shell NM@DMNs (d_4); non-magnetic yolk-shell NM@void@DMNs (c_5); and non-magnetic core-shell DMNs@NM (d_6)

DMSNs。第三，磁性单一材料核壳型M@DMNs和磁性多样材料核壳型M@barrier@DMNs合成过程差异微小，因而在论述中归为一大类。

1 树枝状磁性核壳型纳米反应器研究进展

基于Polshettiwa合成DMSNs的微乳液方法[9]，Yu等在2013年开创性地制备了磁性核@二氧化硅保护层@树枝状二氧化硅壳结构纳米反应器，所得Fe_3O_4@SiO_2@DMSNs对染料的吸附遵循Langmuir等温线规律并符合准二级动力学方程，饱和吸附容量为48.0 mg/g[21]。Nemec等则系统研究了在不同形貌磁性核生长树枝状二氧化硅壳结构的界面共组装技术，制得链状、盘状和球状磁性核壳型纳米反应器(图2a-c)[22]。作者探讨了结构导向剂的正负电性和用量、催化剂的种类和添加量、硅烷前驱体(硅酸四乙酯，TEOS)添加比例、有机相试剂种类等因素对Fe_3O_4@DMSNs形貌以及基本物理化学性能的影响(图$2c_{1-3}$)。基于上述方法能够制备M@barrier@DMNs和M@DMNs，如本课题组使用同一尺寸Fe_3O_4磁性核制备的Fe_3O_4@SiO_2@DMSNs(图2d)和Fe_3O_4@DMSNs(图2e,f)，研究者们设计合成了各式各样功能化纳米反应器用于如下应用领域。

1.1 化学吸附

Emrani等直接使用Fe_3O_4@SiO_2@DMSNs对Cd(II)进行吸附，凭借响应面分析法(RSM)的中心组合设计手段(CCD)研究得出最佳吸附条件为pH=5.9、吸附剂量为1.4 g/L、Cd(II)浓度为59.2 mg/L以及接触时间54分钟[23]。利用DMSNs表面羟基(图2f)可与有机硅烷分子中硅氧烷基团脱水交联成键机制，Goharrizi等将3-巯基丙基三甲氧基硅烷(MPTMS，图$3a_1$)化学接枝于Fe_3O_4@SiO_2@DMSNs表面，产物巯基功能化纳米反应器对Ni(II)、Cd(II)、Cu(II)、Pb(II)和Hg(II)离子的饱和吸附容量依次为33.69、29.58、40.52、44.11和50.56 mg/g[24]。未修饰Fe_3O_4@SiO_2@DMSNs对上述重金属离子饱和吸附容量依次为30.20、23.77、27.84、32.43和36.13 mg/g。所有吸附符合准二级动力学方程并遵循Freundlich等温线规律。该课题组将MPTMS替换为3-氨基丙基三乙氧基硅烷(APTES，图$3a_2$)，制得氨基功能化Fe_3O_4@SiO_2@DMSNs-APTES对上述重金属离子的饱和吸附容量依次为32.71、31.46、30.15、26.52和25.50 mg/g[25]。吸附均自发进行($\Delta G<0$)，符合准二级动力学方程并遵循Freundlich等温线规律。Wang等构筑的Fe_3O_4@SiO_2@DMSNs-APTES在pH为6条件下60分钟达到U(VI)饱和吸附，容量为255.2 mg/g，遵循

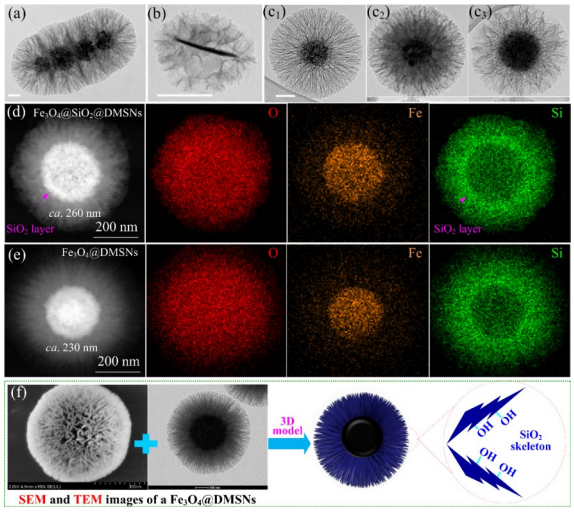

图2　(a-c)链状(a);盘状(b);球状小孔(c_1);球状中孔(c_2)和球状大孔(c_3)树枝状磁性核壳型纳米反应器的透射电镜图[22];(d)本文作者课题组制得Fe_3O_4@SiO_2@DMSNs的透射电镜-元素分布图;(e)本文作者课题组制得Fe_3O_4@DMSNs的透射电镜-元素分布图;(f)由作者课题组制得Fe_3O_4@DMSNs的扫描和透射电镜图像衍生的三维模型示意图

Fig.2　(a) TEM images of magnetic core-shell DMSNs with chainlike (a); disclike (b); and spherical (c) cores; but in forms of small (c_1); medium (c_2); and large (c_3) pores[22]; (d) TEM mapping images of a Fe_3O_4@SiO_2@DMSNs in our laboratory; (e) TEM mapping images of a Fe_3O_4@DMSNs in our laboratory; (f) A three-dimensional model of a Fe_3O_4@DMSNs extracted by its SEM and TEM images

Langmuir等温线规律并符合准二级动力学方程[26]。该课题组在Fe_3O_4@SiO_2@DMSNs表面首先使用3-氰基丙基三甲氧基硅烷(CyPTMS,图3a_3)进行氰基功能化,再通过盐酸羟胺($NH_2OH·HCl$)反应引入偕胺肟(amidoxime, AO)官能团。产物Fe_3O_4@SiO_2@DMSNs-AO在pH为6条件下40分钟快速饱和吸附U(VI),容量为175.4 mg/g,遵循Langmuir等温线规律并符合准二级动力学方程[27]。Lyu等在Fe_3O_4@SiO_2@DMSNs表面接枝正己基三甲氧基硅烷(HTMS,图3a_4)后,疏水性界面饱和吸附乙酸乙酯形成磁性微液滴[28]。含乙酸乙酯的纳米反应器Fe_3O_4@SiO_2@DMSNs-HTMS对水中苯酚、间苯二酚、对苯二甲酸、4-硝基苯甲醛和双酚A有机污染物的去除效率接近100%。Zhang等将Fe_3O_4@SiO_2@DMSNs-APTES加入4-羧基苯硼酸(CPBA)水溶液,在*N*-羟基琥珀酰亚胺(NHS)和1-乙基-(3-二甲基氨基丙基)碳酰二亚胺盐酸盐(EDC·HCl)辅助下室温发生酰化反应[29]。制得苯硼酸功能化纳米反应器Fe_3O_4@SiO_2@DMSNs-CPBA能够在10分钟内饱和吸附邻苯二酚,容量达到293.03 μmol g^{-1}。Yang等将孔道负载Al^{3+}的Fe_3O_4@SiO_2@DMSNs于500 ℃氮气氛围煅烧6小时,制得铝掺杂在树枝状二氧化硅壳层的纳米反应器[30]。其具有强酸活性位点,能够高效去除废水中磷酸盐,吸附容量为12.7 mg/g。

1.2　生物酶的固定及催化

Gao等在Fe_3O_4@DMONs-APTES表面接枝戊二

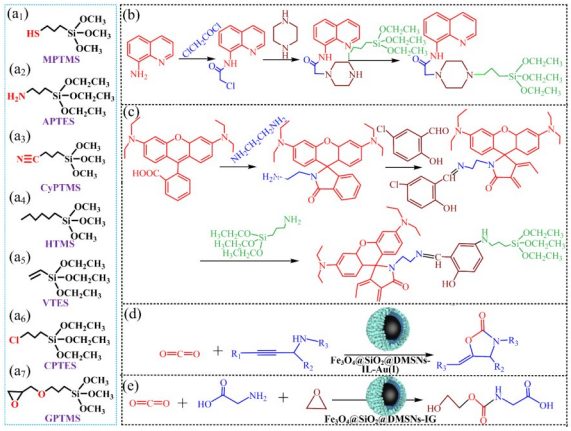

图3　(a)功能化树枝状磁性核壳型纳米反应器的常用硅烷偶联剂;包括3-巯基丙基三甲氧基硅烷MPTMS(a_1);3-氨基丙基三乙氧基硅烷APTES(a_2);3-氰基丙基三甲氧基硅烷CyPTMS(a_3);正己基三甲氧基硅烷HTMS(a_4);乙烯基三乙氧基硅烷VTES(a_5);3-氯丙基三乙氧基硅烷CPTES(a_6)和3-缩水甘油丙氧基三甲氧基硅烷GPTMS(a_7);(b)含8-氨基喹啉官能团的新型硅烷分子合成路线;(c)含罗丹明B官能团的新型硅烷分子合成路线;(d)纳米反应器Fe_3O_4@SiO_2@DMSNs-IL-Au(I)催化系列炔丙胺化合物和二氧化碳生成2-唑烷酮类物质;(e)纳米反应器Fe_3O_4@SiO_2@DMSNs-IG催化CO_2;α-氨基酸和环氧乙烷生成*N*-[(2-羟乙氧基)羰基]甘氨酸

Fig.3　(a) Normal silane coupling agents for functionalization of dendritic magnetic core-shell nanoreactors; including 3-mercaptopropyltrimethoxysilane (a_1); 3-aminopropyltriethoxysilane (a_2); 3-cyanopropyltrimethoxysilane (a_3); hexyltrimethoxysilane (a_4); vinyltriethoxysilane (a_5); 3-chloropropyltriethoxysilane (a_6); and 3-glycidoxypropyltriethoxysilane (a_7); (b) The synthesis route of a novel silane molecule containing 8-aminoquinoline functional group; (c) The synthesis route of a novel silane molecule containing rhodamine B functional group; (d) Synthesis of 2-oxazolidinone with propargylic amines and CO_2 catalyzed by Fe_3O_4@SiO_2@DMSNs-IL-Au(I) nanoreactor; (e) Synthesis of *N*-[(2-hydroxyethoxy)carbonyl]glycine with CO_2; α-amino acid, and ethylene oxide catalyzed by Fe_3O_4@SiO_2@DMSNs-IG nanoreactor

醛(GLU)后固定南极假丝酵母脂肪酶B(CALB),最大载量为93 mg/g,水解活性为22700 U/g[31]。与游离CALB相比,Fe_3O_4@DMONs-CALB展示出超强耐用性和pH稳定性。该纳米反应器能够催化乙酰丙酸和不同链长的脂肪醇进行酯化反应,循环10次后酶催化剂活性保持在85~96%之间。Goharrizi等在Fe_3O_4@SiO_2@DMSNs-APTES表面接枝三聚氯氰(CC)用以固定黄递酶[32]。与游离酶相比,负载酶的纳米反应器展现出大幅增高的耐热性、耐pH性、稳定性、酶活性以及循环利用性能。Ali等在GLU功能化的Fe_3O_4@DMSNs-APTES表面固定假丝酵母脂肪酶(lipase),载量为283 mg/g[33]。与游离lipase相比,Fe_3O_4@DMSNs-lipase相对活性更高(67% > 35%)。28天后,纳米反应器中脂肪酶活性保持原有活性89%,而游离酶仅为原有25%。Qin等利用间苯二酚和甲醛聚合生成酚醛树脂(resorcinol-formaldehyde,RF)反应机制,在Fe_3O_4表面包覆RF有机聚合层(Fe_3O_4@RF)后继续生长DMSNs外壳[17]。采用丙酮抽提技术去除DMSNs结构导向剂(模板剂),形成核壳结构Fe_3O_4@RF@DMSNs。最为重要的是,作者发现搅拌速率决定DMSNs壳孔道大小,搅拌速率越快孔径越大。当DMSNs壳层孔径为9 nm时,尺寸为4 nm的胰蛋白酶(trypsin)载量高达约97 μg/mg。构筑得纳米反应器Fe_3O_4@RF@DMSNs-trypsin对混合蛋白中的低分子量蛋白具有优异选择降解性能,8次循环后材料结构和酶活性依旧稳定。Liu等首先在Fe_3O_4@SiO_2@DMSNs孔道负载氯化物过氧化物酶(CPO)后,通过相变溶菌酶(Phase-Transitioned Lysozyme, PTL)在其表面覆盖一层具备极强黏附力的淀粉样蛋白,然后继续接枝GLU并连接额外一层CPO[34]。目标分子反应器Fe_3O_4@SiO_2@DMSNs-CPO@PTL-CPO能够稳定存于高温有机溶剂,80 °C保留91.3%酶活性,而未固定酶活性同条件处理后仅为37.5%。反应器20分钟内降解诺氟沙星效率达95.2%,而未覆盖外层CPO的Fe_3O_4@SiO_2@DMSNs-CPO纳米反应器降解效率约为88%。

1.3 分析检测及分离纯化

Asghari等在DMSNs合成母液中加入氯吡硫磷(CPF)分子作为模板,在Fe_3O_4@SiO_2磁性核表面共聚生长了DMSNs&CPF杂化壳层[35]。高温煅烧除去CPF和结构导向剂分子后,所得Fe_3O_4@SiO_2@(DMSNs&CPF-void)纳米反应器能够选择性吸收CPF。气相色谱-电子捕获检测技术(GC-ECD)确定CPF含量线性范围及检测限分别为0.003 ~ 0.3和0.001 ng/mL,相对标准偏差(RSD)在4.1 ~ 7.6%之间。Sun等设计合成了一类含有8-氨基喹啉(AQ-silane)的新型硅烷分子(图3b)并将其接枝于Fe_3O_4@SiO_2@DMSNs[36]。所得Fe_3O_4@SiO_2@DMSNs-AQ能选择性识别Zn(II),缔合常数和检测限分别为1.85×10^5 M^{-1}和1.08×10^{-7} M。Radhakrishnan等设计合成了一类含有罗丹明B(RB)的新型硅烷分子(图3c)并将其接枝于Fe_3O_4@MnO_2@SiO_2@DMSNs表面[37]。构筑得纳米反应器Fe_3O_4@MnO_2@SiO_2@DMSNs-RB能够定向识别Cu(II),吸附产物在569 nm产生荧光增强现象,检测限为12.3×10^{-8} mol。采用相似有机合成机理,该课题组还设计合成了一类含有1-芘甲醛(PC)的新型硅烷分子并将其接枝于$CoFe_2O_4$@SiO_2@DMSNs表面[38]。产物$CoFe_2O_4$@SiO_2@DMSNs-PC能够特异识别Hg(II),吸附材料在456 nm产生荧光增强现象,检测限为4.1×10^{-9} mol,线性度良好(R^2=0.9906)。Zhao等在Fe_3O_4@DMSNs表面依次化学修饰乙烯基三乙氧基硅烷(VTES,图$3a_5$)和3-巯基-1-丙磺酸钠(MPS)[39]。所得-SO_3^-功能化Fe_3O_4@DMSNs-(VTES&MPS)通过静电作用吸附含对苯二硼酸(DBA)官能团的季铵盐,所得纳米反应器通过硼羟基特异吸附糖化物(saccharide)。采用氨水破坏复合体系界面电荷平衡后,苯二硼酸-糖化物(DBA-saccharide)复合物从磁性反应器表面脱离。紫外可见光谱联合高效液相色谱可检测DBA-saccharide中糖种类及含量,精确度达80 ~ 100%。Gao等在Fe_3O_4@DMONs-APTES-GLU表面接枝*N*,*N*-双(羧甲基)-*L*-赖氨酸后负载Ni(II),产物能够吸附ω-转氨酶(ω-TA)[40]。未固定ω-TA最佳吸附pH为7.5,Fe_3O_4@DMONs-Ni(II)最佳吸附pH为7。纳米反应器负载的生物酶展现出更优异的热稳定性、耐酸碱性和储存性能,循环利用12次后活性依旧为初始67.38%。Hong等人在Fe_3O_4@RF@DMSNs表面层层自组装聚乙烯亚胺(PEI)、植酸(PA)和$Ti(SO_4)_2$,得到双功能Fe_3O_4@RF@DMSNs-PEI-PA-Ti^{4+}[41]。该纳米反应器既能作为亲水相互作用色谱(HILIC)材料富集*N*-糖肽结合蛋白,又可作为固定化金属离子亲和色谱(IMAC)材料富集磷酸肽。Jin等将1,3,5-三甲基六氢-1,3,5-三嗪(TMTA)和1,5-萘二酚(DHN)浸入Fe_3O_4@SiO_2@DMSNs孔道,45 °C温育1.5小时制得π-共轭聚合物(π-CP)负载于孔道的纳米

反应器[42]。以该Fe_3O_4@SiO_2@DMSNs-(π-CP)为高效液相色谱(HPLC)的固相萃取材料,成功建立了快速灵敏检测季铵型生物碱(QAAs)的分析方法。

1.4 PNIPAM接枝开关膜的制备

Dong等将MPTMS替换为3-巯基丙基三乙氧基硅烷(MPTES,图3a_1中的甲氧基替换为乙氧基),制得巯基功能化γ-Fe_2O_3@SiO_2@DMSNs-MPTES。在其孔道吸附Au(III)离子并用硼氢化钠还原后,得到Au纳米粒子负载的树枝状磁性核壳纳米反应器[43]。其作为催化剂在360秒完全还原对硝基苯酚,表观速率常数为1.45×10^{-2}/s,6次循环后性能基本不变。Sun等人采用类似方法制得Fe_3O_4@SiO_2@DMSNs-APTES-Ag在紫外照射下7分钟内能够有效降解对硝基苯酚和邻硝基苯胺,反应速率分别为0.87和0.52/min[44]。Sadeghzadeh在Fe_3O_4@SiO_2@DMSNs表面依次接枝3-氯丙基三乙氧基硅烷(CPTES,图3a_6)和双四唑亚甲基芳烃类化合物,形成离子液体修饰的磁性核壳复合材料[45]。进一步负载Au离子得到Fe_3O_4@SiO_2@DMSNs-IL-Au(I),该纳米反应器能催化系列炔丙胺化合物和二氧化碳生成2-唑烷酮类物质(图3d)。10次循环后,仅有0.2 ppm的Au脱离催化剂,催化效率略微下降。该课题组在树枝状磁性核壳型纳米粒子设计合成及催化应用方面开展了大量工作[46-53],制备了氨基倍半硅氧烷(POSS-NH_2)以及Salen配体(由伯二胺和水杨醛类化合物制得的螯合配体,与金属离子形成稳定络合物)修饰的催化剂反应器,如Fe_3O_4@SiO_2@DMSNs-POSS/salen/Pd(II)[49]、$FeNi_3$@SiO_2@DMSNs-POSS@Salen/Cu(II)[50]、$FeNi_3$@SiO_2@DMSNs- salen/Pd(II)[51]等。Zhang等在Fe_3O_4@DMSNs孔道吸附钨酸钠和硝酸铋溶液后,于180 ℃水热反应合成Bi_2WO_6负载的Fe_3O_4@DMSNs-Bi_2WO_6[54]。该纳米反应器在可见光照射下4小时降解83%亚甲基蓝,4次循环后效率基本保持不变。Zhiani等在Fe_3O_4@SiO_2@DMSNs孔道依次吸附螺旋藻和三聚磷酸钠,反应生成离子凝胶(IG)修饰的Fe_3O_4@SiO_2@DMSNs-IG[55]。该纳米反应器能催化CO_2、α-氨基酸和环氧乙烷生成*N*-[(2-羟乙氧基)羰基]甘氨酸(图3e),产率达到97%,10次循环后降至95%。该课题组还设计构筑了$FeNi_3$@SiO_2@DMSNs-IG-Pd纳米反应器,催化CO_2、丙炔醇和仲胺类化合物生成β-氧代丙基氨基甲酸酯[56]。Galehban等设计构筑的Fe_3O_4@SiO_2@DMSNs-MPTES-Cu(II)纳米反应器,不仅能够还原对硝基苯酚,加速苯甲醛和4-羟基香豆精生成双香豆素类化合物[57],还可以催化苯甲醛类化合物和2-氨基苯甲酰胺绿色合成2-芳基-2,3-二氢-4(1*H*)-喹唑啉酮类有机物[58]。Saberi等首先在$FeNi_3$@SiO_2@DMSNs表面接枝3-缩水甘油丙氧基三甲氧基硅烷(GPTMS,图3a_7),然后利用三元环氧基团易与多种试剂发生开环反应机制,继续接枝2,2,6,6-四甲基哌啶-1-氧自由基(TEMPO)和漆酶后,制得能够高效降解系列芳香族硝基制药类有机污染物的纳米反应器[59]。Seo等在Fe_3O_4@DMSNs孔道吸附钛酸四丁酯(TBOT)并高温煅烧后,得到锐钛矿TiO_2纳米粒子负载的Fe_3O_4@DMSNs-TiO_2,该纳米反应器展现出优于商业P25的亚甲基蓝降解性能[60]。Wei等在Fe_3O_4@DMSNs-Pt表面化学接枝甲基三甲氧基硅烷,构得疏水化改性双相催化剂[61]。该纳米反应器Fe_3O_4@DMSNs-Pt/CH_3能够在2小时内100%高效催化还原硝基苯为氨基苯,而未疏水化处理的Fe_3O_4@DMSNs-Pt同条件转化率仅为39%。Qiu等使用钛酸四异丙酯包覆Fe_3O_4后继续增长树枝状二氧化硅壳层,高温煅烧得到锐钛矿TiO_2包覆磁性核的Fe_3O_4@TiO_2@DMSNs[62]。相较于商业P25,纳米反应器展现出优越的有机氯类和双酚A化合物降解性能。

1.5 药物递送及生物治疗

Gu等在椭圆形赤铁矿(Fe_2O_3)表面构筑DMSNs(Fe_2O_3@DMSNs,图4a_1),经H_2/N_2煅烧生成椭圆形Fe_3O_4@DMSNs(图4a_2)[63]。将上述2类纳米反应器放入未成熟巨噬细胞,Fe_2O_3@DMSNs对细胞的活化性能劣于Fe_3O_4@DMSNs,归因于前者在缓冲环境释放铁的速率慢。Atabaev等在DMSNs合成母液加入荧光素,制得染料掺杂于树枝状壳层的功能化Fe_3O_4@(DMSNs&dye)[64]。体外实验表明,当该纳米反应器浓度小于10 ppm,对细胞基本无害,之后毒性随浓度增大而变大。因此,在低浓度范围能够将药物负载于Fe_3O_4@(DMSNs&dye)孔道并进行递送,可联用荧光技术监测运输过程。Chen等首先在FeOOH纳米柱表面包覆DMSNs,构筑了与图4a具有相似椭圆形结构的FeOOH@DMSNs,经过H_2/N_2煅烧形成部分铁被还原的椭圆形(Fe&Fe_3O_4)@DMSNs[65]。再将过氧化氢酶(CAT)负载于树枝状孔道并用聚多巴胺(PDA)层包覆后,溶液抽提除去CAT制得(Fe&Fe_3O_4)@DMSNs-void-PDA作为CAT印迹材料。体外实验表明:纳米反应器选择抑制肿瘤细胞中的

CAT生物活性。此外，(Fe&Fe_3O_4)核中的铁参与Fenton反应催化H_2O_2生成羟基自由基(·OH)，结合近红外光(NIR)光热技术，(Fe&Fe_3O_4)@DMSNs-void-PDA能高效灭除MCF-7、HeLa和293T肿瘤细胞。Fiedler等在超顺磁氧化铁纳米粒子(SPION)表面构筑DMSNs壳层，探讨了TEOS用量对SPION@DMSNs粒径、壳厚度及壳密度的影响(图4b)，揭示出具有不同壳密度的SPION@DMSNs在模拟体液中硅壳降解动力学规律，并最终证明SPION@DMSNs是一种可控药物递送载体平台[66]。

1.6 超湿润界面

Alamri等在Fe_3O_4@SiO_2@DMSNs、Fe_3O_4@SiO_2和DMSNs表面化学修饰正辛基三甲氧基硅烷(TMOS)[67]。将制得的3种粒子涂覆于环氧树脂覆盖的不锈钢基底，得到界面接触角分别为175°，135°和154°。Fe_3O_4@SiO_2@DMSNs-TMOS具有优越的耐酸、碱和盐溶液性能。本文作者课题组在具有不同孔径的Fe_3O_4@DMSNs表面接枝正十八烷基三乙氧基硅烷(OTES)，制得孔径依次为10、25和60 nm的超疏水Fe_3O_4@DMSNs-OTES(图4c)[68]。水滴在3类纳米反应器形成平面的接触角分别为152°、154°和158°。3类纳米反应器形成的磁液珠接触角均大于160°，能高效去除乳液中的油成分。小孔径反应器(图$4c_1$)去除速率最快，中型孔径反应器(图$4c_2$)吸附量最大。Wang等在DMSNs合成母液中加入OTMS，通过共聚法制备了Fe_3O_4@(DMSNs&ODMS)超疏水纳米粒子[69]。与不具有树枝状纹理的介孔纳米颗粒Fe_3O_4@(MSNs&ODMS)相比，Fe_3O_4@(DMSNs&ODMS)纳米反应器水接触角更大(155° > 140°)，具有更高的油吸附容量(如石油醚吸附量为2.04 > 1.02 g/g)。

2 树枝状蛋黄-蛋壳型纳米反应器研究进展

2.1 磁性树枝状蛋黄-蛋壳型

如前所述，Qin等对Fe_3O_4@RF@DMSNs采用丙酮抽提技术去除DMSNs结构导向剂形成核壳结构[17]。该团队还将Fe_3O_4@RF@DMSNs于空气中500 °C煅烧5小时，构筑得磁性蛋黄@中空空间@二氧化硅蛋壳纳米反应器(图4d)。Ali等煅烧Fe_3O_4@SiO_2@RF@DMSNs构筑了Fe_3O_4@SiO_2@void@DMSNs蛋黄-蛋壳结构[70]。继续依次化学接枝APTES和GLU后，便可固定皱褶假丝酵母脂肪酶(CRL)。纳米反应器Fe_3O_4@SiO_2@void@DMSNs-CRL展示出优越的负载能力、活性、热稳定性和耐酸碱性。

2.2 非磁性树枝状蛋黄-蛋壳型

2.2.1 *树枝状结构为壳层* Bian等开发了一锅自模板界面扩散法制备DMSNs空心球技术[71]。有趣的是，在合成目标产物的过程中，出现了硅烷前驱体为蛋黄、二氧化硅为蛋壳的过渡结构。如图4e所示，TEM图分别为反应在10、18和24小时(终点)对应的核壳、蛋黄-蛋壳和空心结构。Yang等在介孔有机硅球(mesoporous organosilica nanoparticles, MONs)表面构筑DMONs壳层，利用壳层中有机硅和无机硅的不同组成梯度[72]，刻蚀去除壳层内部无机硅组成，制得非磁性蛋黄-蛋壳MONs@void@DMONs(图4f)[73]。将小分子前体药物巴诺蒽醌(AQ4N)和葡萄糖氧化酶(GOx)分别负载于纳米反应器中心核MONs与外壳DMONs。通过细胞内谷胱甘肽(GSH)氧化还原反应致使壳层中有机硅的硫-硫键断裂，促使壳层快速降解并释放GOx。GOx氧化葡萄糖，削弱肿瘤能量供给并产生活性氧引发氧化损伤。缺氧环境激活AQ4N形成有毒拓扑异构酶II抑制剂(AQ4)，从而产生强效细胞毒性抑制肿瘤生长。

2.2.2 *树枝状结构为中心核* Du等以孔道嵌入贵金属纳米粒子(Au或Pt，以前者为例)的树枝状结构为中心核，设计构筑了(DMSNs-APTES-Au)@RF@MSNs(mesoporous silica nanoparticles, MSNs)核壳结构[74]。空气中煅烧除去RF及结构导向剂后，得到(DMSNs-APTES-Au)@void@MSNs蛋黄-蛋壳构型纳米粒子(图4g)。通过控制结构导向剂CTAB和二氧化硅前驱体TEOS添加量，便可制备厚度为35、60和95 nm的MSNs壳层。与具有60和95 nm壳厚的纳米反应器相比，35 nm壳厚反应器能够更加快速催化还原对硝基苯酚为对氨基苯酚。与没有MSNs壳层的DMSNs-APTES-Au相比，蛋黄-蛋壳构型反应器耐酸性和耐用性大幅提升。作者还研究了纳米反应器对环辛烯的催化环氧化作用，底物的转化率达98%，产物1,2-环氧基环辛烷、烯酮和烯醇的选择性依次为82%、6%和5%。该纳米反应器也能够出色催化氧化苯乙烯生成环氧基苯乙烷、苯乙醛和苯甲醛，底物的转化率达99%。但是随着反应温度升高，环氧基苯乙烷选择性降低，苯甲醛选择性增高。上述课题组以(DMSNs-APTES-Au)@RF为

研究对象，使用强碱将二氧化硅DMSNs部分刻蚀去除得到(Void-Au)@RF中空结构，或先将RF在惰性环境煅烧转化为碳层(C)后再使用强碱刻蚀二氧化硅得到(Void-Au)@C中空结构[75]。(Void-Au)@RF在8分钟内完全催化还原对硝基苯酚，速率常数为0.215/min。而(Void-Au)@C催化时间更长，速率常数仅为0.059/min，远小于(Void-Au)@RF纳米反应器。

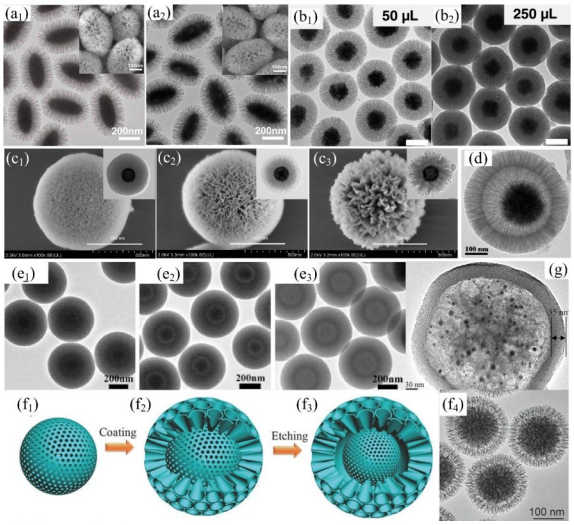

图4　(a) 椭圆形树枝状核壳结构的透射和扫描电镜图；包括Fe_2O_3@DMSNs(a_1)和Fe_3O_4@DMSNs(a_2)[65]；(b) 通过调节TEOS添加量制得不同粒径和孔密度SPION@DMSNs的透射电镜图[66]；(c) 本文作者课题组制得具有10、25和60 nm孔径Fe_3O_4@DMSNs-OTES的透射和扫描电镜图；(d) 蛋黄-蛋壳结构Fe_3O_4@SiO_2@void@DMSNs的透射电镜图[17]；(e) 一锅自模板界面扩散法制得核壳、蛋黄-蛋壳和空心结构DMSNs的透射电镜图[71]；(f) 蛋黄-蛋壳型MONs@void@DMONs的合成示意图及其透射电镜图[73]；(g) DMSNs为中心核制备得(DMSNs-APTES-Au)@void@MSNs的透射电镜图[74]

Fig.4　(a) TEM and inserted SEM images of elliptical magnetic core-shell architectures; being Fe_2O_3@DMSNs (a_1) and Fe_3O_4@DMSNs (a_2)[65]; (b) TEM images of SPION@DMSNs with various diameters and pore densities adjusted by TEOS dosage[66]; (c) TEM and inserted SEM images of superhydrophobic Fe_3O_4@DMSNs-OTES with 10, 25, and 60 nm pores prepared in our laboratory; (d) TEM image of yolk-shell Fe_3O_4@SiO_2@void@DMSNs[17]; (e) TEM images of core-shell, yolk-shell, and hollow DMSNs prepared by a one-pot self-templated interfacial diffusion method[71]; (f) Schematic illustration of the synthesis process of MONs@void@DMONs and its TEM image[73]; (g) TEM image of a (DMSNs-APTES-Au)@void@MSNs nanoreactor[74]

3　树枝状非磁性核壳型纳米反应器研究进展

3.1　树枝状结构为壳

基于DMSNs的微乳液制备方法[9]，Moon等揭示DMSNs特异形貌在Winsor III型乳液体系完成(图5a)[76]。通过调节反应参数，以无定型二氧化硅纳米球或DMSNs为中心核、DMSNs为外壳的系列SiO_2@DMSNs和DMSNs@DMSNs复合体被合成。此外，研究发现助溶剂种类(异丙醇、正丁醇或正戊醇)能够调控壳层形貌和孔道大小。Qu等揭示SiO_2@DMSNs壳层结构不以连续方式逐步生长，而以不连续阶梯式方式形成外部多孔宏观结构[77]。不同搅拌速率引起的TEOS水解缩合速率以及表面活性剂形成的胶束结构差异，促使壳层厚度和孔径发生变化。作者推测SiO_2@DMSNs形成机制分为如下步骤(图5b)：(1)搅拌扰动油相与水相界面；(2)表面活性剂分子在扰动界面由线性排列变为弯曲型；(3)弯曲排列的表面活性剂分子形成胶束进入油相或水相；(4)扰动的油水两相界面导致进入油相的胶束在表面活性剂分子的包裹下重新进入水相中，反之亦然；(5)重新进入水相或油相的胶束变形为囊泡结构，同时TEOS与囊泡中的水混合进行水解反应；(6)TEOS水解形成的硅酸分子集中至胶束极性头部，后经过协同组装形成特异放射状孔道结构。Dai等凭借微乳液法将DMSNs生长于上转换纳米颗粒(UCNPs)表面，调整助表面活性剂(正丁醇)添加量可控制壳层孔径分布在10 ~ 40 nm范围[78]。纳米反应器UCNPs@DMSNs具有特异自吸附性能，约10 nm的$Cu_{1.8}S$、Au以及25 nm Fe_3O_4粒子能够自主吸附负载于其孔道。

赵东元院士课题组于2014年开发油水双相分层技术来合成单分散、粒径均匀的DMSNs、DMSNs@DMSNs或DMSNs@DMSNs@DMSNs多层级结构(图5c-e)[79]。TEOS分散在体系上部油相，表面活性剂和催化剂分散在下部水相。通过改变油相溶剂类型(十八烯、十氢萘或环己烷)、TEOS浓度、反应时间等因素，便可调控DMSNs孔径分布于2.8 ~ 13 nm范围，DMSNs壳层厚度处于5 ~ 180 nm。双相分层界面组装和生长过程机制表明：半胶束和硅酸低聚物自组装成为介孔结构，油分子通过影响界面组装调控孔径尺寸(图5f)。得益于其优异的生物兼容性、可调孔径和多级结构，单层和多层核壳

DMSNs被证明是一种具有应用前景的蛋白质递送纳米反应器。

3.1.1 催化合成与降解 Jalil等在树枝状非磁性核壳纳米反应器设计构筑及工业化应用方面做了大量工作[80-97]。以分子筛ZSM-5、BEA、zeolite、丝光沸石(mordenite)及介孔材料SBA-15为中心核,制得纳米反应器ZSM-5@DMSNs-Pt用于催化异丙基苯加氢裂化[80]、质子化ZSM-5@DMSNs(HZSM-5@DMSNs)提高苯与甲醇烷基化反应的产物选择性和机理揭示[81-82]、ZSM-5@DMSNs催化CO甲烷化的热力学和机理探究[83-84]、ZSM-5@DMSNs-TiO_2光催化降解醋氨酚[85]、ZSM-5@DMSNs-Ni以及ZSM-5@DMSNs-(Ni&M)(M=Mg、Ca、Ta或Ga)促进甲烷干重整反应[86]、mordenite@DMSNs催化CO或CO_2甲烷化[87-88]、质子化BEA@DMSNs(HBEA@DMSNs)加速C_6烷烃和环烷烃的分子异构化[89]、BEA@DMSNs促进甲苯和甲醇生成二甲苯类化工制品[90]、BEA@DMSNs高效催化CO甲烷化生产代用天然气(SNG)[91]、Zeolite-Y@DMSNs-Pt催化十二烷加氢异构化[92]、质子化Zeolite-Y@DMSNs-Pt催化有机C5~C7化合物的分子异构化[93]、SBA-15@DMSNs合成细节对核壳结构的形貌调控[94]、SBA-15@DMSNs-Ni促进甲烷干重整[95-96]、SBA-15@DMSNs-Fe_2O_3光催化降解亚甲基蓝[97]等。

赵东元院士课题组以近似正方形的LTA分子筛纳米晶(ZeoA)为中心核,通过油水双相分层技术构筑了ZeoA@DMSNs核壳结构[98]。该单分散性球形纳米反应器壳层具有2~10 nm的中心径向梯度介孔,中心核具有0.5 nm均匀微孔(图5g)。通过调整自组装复合胶束模板基本单元,可以精确控制DMSNs介孔尺寸。分层梯度多孔结构完美模拟自然界分层多孔系统,表现出溶液自发快速传质到内部化学反应活性位点这一特性,正如毛细管的导向作用。ZeoA@DMSNs催化长链羧基棕榈酸酯化反应产率达到75%,即使在水干扰下稳定性依旧极高。ZeoA核和梯度多孔壳结构能够高效捕水并将其从DMSNs壳快速传输到ZeoA内芯,进而推动化学平衡。ZeoA@DMSNs-Pd对甲基吲哚的C-H芳基化反应催化转化率高达98%。与无沸石核的DMSNs-Pd相比,其耐水性能显著提高26%。Peng等在长方体状钛硅分子筛TS-1表面生长树枝状二氧化硅壳制得椭球形TS-1@DMSNs,然后将$Rh(OH)_3$负载于孔道形成TS-1@DMSNs-$Rh(OH)_3$催化剂[99]。

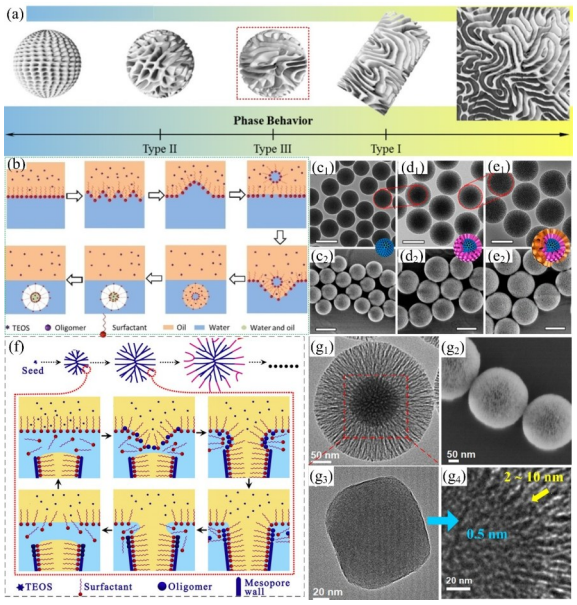

图5 (a)具有不同相行为和微结构的水-表面活性剂-油三相系统[76];(b)扰动界面形成SiO_2@DMSNs机制示意图[77];(c)DMSNs;(d)DMSNs@DMSNs和(e)DMSNs@DMSNs@DMSNs;纳米颗粒的透射(c_1-e_1);扫描(c_2-e_2)电镜图及三维模型图[79];(f)双相分层法合成DMSNs的界面增长机制[79];(g)ZeoA@DMSNs的透射(g_1)和扫描(g_2)电镜图。ZeoA(g_3)以及ZeoA核-DMSNs壳交汇界面(g_4)的透射电镜图[98]

Fig.5 (a) Water-surfactant-oil ternary systems with various phase behaviors and substructures[76]; (b) Schematic illustration of formation mechanism of SiO_2@DMSNs from the disturbed interface[77]; (c-d) TEM (c_1-e_1); SEM (c_2-e_2); and inserted 3D model images of DMSNs (c); DMSNs@DMSNs (d); and DMSNs@DMSNs@DMSNs (e)[79]; (f) Synthesis mechanism of DMSNs by interfacial growth from biphase stratification approach[79]; (g) TEM (g_1) and SEM (g_2) images of ZeoA@DMSNs; TEM images of ZeoA (g_3) and the boundary between ZeoA core and DMSNs shell (g_4)[98]

研究发现该纳米反应器能高效催化苯甲醛、氨和过氧化氢合成苯甲酰胺。该课题组详细研究了反应温度、时间、TEOS和TS-1摩尔比、有机相比例等因素对TS-1@DMSNs形貌结构的影响,以及不同醛类底物的转化率和产物选择性能[100]。Awad等考察了3~15 wt%镍负载量的La_2O_3@DMSNs-Ni对甲烷干重整反应的催化性能影响[101]。Shabir等合成了SiO_2@DMSNs-Ag用于催化还原硝基化合物和降解染料[102]。

3.1.2 分析检测及分离纯化 安徽建筑大学瞿其曙教授团队在SiO_2@DMSNs类材料的合成工艺以及其作为高效分离介质材料的应用领域方面开展了大量工作[103-108]。基于DMSNs的微乳液制备方法[9],

通过控制搅拌速率和助溶剂种类(异丙醇、正丁醇或正戊醇),该团队构筑了系列SiO_2@DMSNs,壳厚在13 ~ 67 nm范围可控,孔径能够处于5 ~ 16 nm,而粒径可从500 nm增长至3 μm[103]。将用长链硅烷OTES改性制得的疏水SiO_2@DMSNs-OTES用作高效液相色谱(HPLC)填充材料,有机萘化合物分离理论塔板数高达2.25×10^5 plates m^{-1},被压低至5.8 MPa。作者课题组探讨了十八胺(ODA)作为模板剂对SiO_2@DMSNs的形貌结构影响。随着ODA添加量增加(0.1 →1.0 g),DMSNs孔径从7.1增至22.3 nm[104]。改性疏水SiO_2@DMSNs-OTES分离二甲基萘化合物的理论塔板数达219789 plates/m。上述课题组还揭示了油相类型(环已烷、甲苯、苯、二甲基苯胺和乙酸乙酯)对SiO_2@DMSNs形貌结构的影响,不同油相使得DMSNs孔径在7 ~ 37 nm范围可调[105]。SiO_2@DMSNs纳米反应器能快速分离小分子、肽类化合物、小分子蛋白和分子量高达200 KDa的大分子蛋白,有机劳化合物分离理论塔板数达264531 plates/m。此外,该团队先在SiO_2@DMSNs-APTES表面接枝戊二酐生成羧基功能化SiO_2@DMSNs核壳结构,中间产物SiO_2@DMSNs-COOH的孔道继续负载$Zn(NO_3)_2 \cdot 6H_2O$和2-甲基咪唑前驱体后,室温孵化24小时制得金属有机框架(ZIF-8)修饰的纳米反应器SiO_2@DMSNs-ZIF[106]。通过控制反应溶剂体积,ZIF-8可调控为约3.4 nm的薄层覆盖于球体界面而非微晶颗粒负载于孔道内部。SiO_2@DMSNs-ZIF对二甲苯异构体的分离理论塔板数高达2.1×10^5 plates/m。将TBOT前驱体吸附于SiO_2@DMSNs孔道并煅烧,便制得TiO_2修饰的SiO_2@DMSNs-TiO_2[107]。该反应器特有的7 nm孔道不能够吸附大尺寸蛋白,TiO_2界面通过配位作用特异吸附磷酸肽,故而能提高毛细管电泳-质谱联用仪对磷酸肽鉴定的灵敏性,检测限低至浓度为1.0 fmol/μL。上述课题组还将SiO_2@DMSNs-TiO_2用于婴幼儿食品中含磷氨基酸型除草剂(PAAHs)的提取富集分析[108]。以草甘膦、草铵膦及其主要代谢物(氨甲基膦酸和3-甲基膦丙酸)作为分析物,纳米反应器中TiO_2界面和磷酸盐特异吸附,定量下限为0.3 ~ 1.6 ng/mL。所建立分析方法对9种商业婴幼儿食品进行检测,分析物平均回收率在82.3 ~ 102.6%之间,5次实验RSD在2.1 ~ 8.3%范围内。

Wang等将聚苯胺(PANI)化学修饰于SiO_2@DMSNs表面,所得SiO_2@DMSNs-PANI能够富集和纯化苯甲酮类紫外线吸收剂[109]。联合毛细管电泳-质谱技术,纳米反应器成功检出6类苯甲酮类紫外线吸收剂,检出限范围在0.6 pg/mL ~ 0.2 ng/mL之间,浓缩因子介于470 ~ 660。Zhang等在3 μm二氧化硅球表面生长了孔径为19.9 nm、壳厚为50 ~ 100 nm的DMSNs,疏水改性得SiO_2@DMSNs-OTES作为HPLC固定相介质能够高效分离小分子和蛋白质[110]。当介质流速为1.0 mL/min时,被压低至8.5 MPa。当壳层厚度为80 nm时,反应器能在10分钟分离7种小分子,6分钟分离6类蛋白质。Siddiki等首先制备了ZnO_2和钬(Ho)掺杂的ZnO_2&Ho纳米颗粒,以此为中心核构筑ZnO_2@DMSNs和(ZnO_2&Ho)@DMSNs核壳结构[111]。激光扫描共聚焦荧光显微镜结果表明:DMSNs壳层优异的防护作用使得两类粒子荧光性能一年内无法淬灭。作者展望Ho掺杂的纳米反应器能够被中子活化($^{165}Ho \rightarrow ^{166}Ho$),可用于生物成像及生物治疗。Wang等首先在DMSNs合成母液中添加了VTES,构筑了乙烯基团修饰的SiO_2@(DMSNs&VTES),再通过谷胱甘肽GSH含有的巯基和乙烯基进行硫醇-烯点击化学反应,成功将GSH接枝于核壳结构表面[112]。作为亲水色谱固定相,SiO_2@DMSNs-GSH短程有序孔道显著提升传质效率。2分钟内从大鼠肝脏蛋白酶解液中富集2186条*N*-糖肽(对应806种糖蛋白),与1小时富集完毕的糖蛋白和糖肽重叠率分别达88.3%和79.1%。Sun等在SiO_2@DMSNs合成过程对SiO_2中心核和DMSNs外壳合成母液分别加入$CsPbBr_3$前驱体和CdTe量子点(QDs)进行掺杂,并在杂化中心核额外包覆一层$CsPbBr_3$[113]。所构$CsPbBr_3$和CdTe量子点封装的纳米反应器(SiO_2&$CsPbBr_3$)@$CsPbBr_3$@(DMSNs&CdTe)被用作双发射荧光温度探针,通过监测两种QDs荧光峰强度变化比或波长间距偏移值从而实现温度感知测定。

3.1.3 *药物递送及生物治疗* 哈尔滨工程大学杨飘萍教授课题组在UCNPs@DMSNs孔道依次负载S-亚硝基硫醇(SNO)、过氧化铜(CuO_2)和光敏剂二氢卟吩(Ce6)后,将聚乙二醇(PEG)共价结合在纳米反应器表面进行封端[114]。UCNPs@DMSNs-SNO-(CuO_2&Ce6)-PEG进入肿瘤细胞进行化学动力学(CDT)治疗、NIR诱导的光动力疗法(PDT)和气体治疗。CDT体现在肿瘤细胞微酸性环境促使CuO_2分解,Cu^{2+}和GSH反应生成Cu^+,H_2O_2与Cu^+作用生成羟基自由基(·OH)。PDT过程表现为除了纳米反应器

在NIR作用下产生单线态氧($^1O_2$)外，Cu^{2+}还与SNO反应生成NO。气体治疗为NO和活性氧物质(ROS，$^1O_2$和·OH)生成活性氮类(RNS)。此外，UCNPs中的镧系元素赋予纳米反应器上转换发光(UCL)、断层扫描(CT)和磁共振成像(MRI)三模态成像性能。该课题组将MoO_x负载于以下转换纳米颗粒(DCNPs)为中心核制备的DCNPs@DMSNs粒子孔道并进行PEG封端[115]。纳米反应器DCNPs@DMSNs-MoOx-PEG在808 nm激光射下通过下转换发光机制产生两个明显的近红外二区(NIR-II)窗口发射峰：1060 nm和1300 nm。在肿瘤细胞微酸性环境，MoO_x和H_2O_2反应生成$^1O_2$(促进低氧)，存在的GSH也被Mo催化消耗。DCNPs中钆离子和钇离子赋予纳米粒子计算机断层(CT)和MRI成像功能。基于镧系元素掺杂的UCNPs@DMSNs和DCNPs@DMSNs核壳结构，上述团队将Au纳米粒子负载于壳层孔道后用$CaCO_3$层封端[116]。在980 nm光激发下，UCNPs-或DCNPs@DMSNs-Au@$CaCO_3$实现近红外二区1550 nm和可见光540 nm产生强发射。在肿瘤酸性环境，$CaCO_3$复分解产生CO_2气泡。上述作用都会产生并增强光声成像(PAI)和荧光成像(FI)，有利于肿瘤的精确诊断。杨飘萍教授团队还设计构筑了以柱状Bi_2S_3为中心核，树枝状结构为外壳的椭球状Bi_2S_3@DMSNs-APTES(图6a)[117]。将2-溴-2-甲基丙酸(BMPA)化学改性的CeO_2纳米酶负载于壳层孔道并以PEG封端，所得Bi_2S_3@DMSNs-CeO_2-PEG纳米反应器在NIR-II产生过高热、活性氧物质(O_2和·OH)，外加消耗GSH达到肿瘤消融治疗作用。凭借Bi元素的超高X射线衰减性能，反应器能够实现高对比CT成像。

澳大利亚昆士兰大学余承忠教授课题组等以富勒烯(C_{60})掺杂的二氧化硅杂化球为中心核，构筑了(SiO_2&C_{60})@DMSNs-OTES纳米反应器[118]。杂化SiO_2&C_{60}作为光敏剂和荧光成像剂，疏水改性的DMSNs-OTES壳层用以装载抗磷酸化Akt单克隆抗体(mAb anti-pAkt)。当(SiO_2&C_{60})@DMSNs-pAkt被递送至细胞，在紫外照射下杂化SiO_2&C_{60}产生荧光并生成单态氧($^1O_2$)；anti-pAkt通过阻塞pAkt和抗凋亡Bcl-2蛋白抑制细胞生长。纳米反应器结合了PDT和抗体疗法，有效阻止人类乳腺癌细胞MCF-7增长。Wan等在MSNs@DMSNs-Pt孔道负载尿激酶(UK)和抗凝血药肝素(Hep)后，用血小板膜(PM)包覆复合纳米粒子得到MSNs@(DMSNs-Pt&UK&Hep)@PM[119]。在PM特殊蛋白的调控下，纳米反应器定向移动至血栓位置，NIR激发PM破裂并快速释放UK(3小时)和长效释放Hep(20天)，从而实现溶栓疗法。该课题组还在MSNs@DMSNs-Pt孔道负载DOX和抗癌药物肝素-叶酸(HF)复合物，其中DOX进入MSNs微孔而HF进入DMSNs大孔[120]。凭借表面等离子体共振(SPR)效应，Pt在NIR作用下产生的热量驱动MSNs@(DMSNs-Pt&DOX&HF)释放药物抑制肿瘤细胞增长，实现光驱动的药物治疗和光热治疗。Liu等在氨基功能化CuS@DMSNs-APTES孔道负载Hep，再通过Schiff碱反应将氧化透明质酸(OHA)接枝于表面封端[121]。具有pH响应性能的CuS@DMSNs-Hep-OHA在动脉硬化弱酸性环境可控释放Hep，CuS在NIR作用下将光转为热能，化学和光热协同高效治疗动脉硬化。Xu等首先制备了金纳米柱(GNRs)为中心核的GNRs@(DMSNs&MPTMS)，然后将聚乙二醇化的核壳结构负载阿霉素(DOX)[122]。经^{89}Zr标记后，GNRs@DMSNs-DOX被用于正电子发射断层显像(PET)和光声(PA)影像介导的活体化疗-光热治疗。PET和PA结果表明：增强渗透与滞留(EPR)效应促使纳米反应器趋于肿瘤区域，达到理想治疗效果。Wang等在氨基功能化UCNPs@DMSNs-APTES孔道负载卡那霉素掺杂的碳纳米点(KCQs)和一氧化氮供体BNN6[123]。所得UCNPs@DMSNs-(KCQs&BNN6)纳米反应器在NIR照射下产生超氧阴离子和NO，两者反应生成能够损害活细胞的过氧亚硝基阴离子($ONOO^-$)，进而对糖尿病伤口进行抗感染治疗。Sadabad等制备的TaO_x@DMSNs-MPTMS-Au具有良好的毒性特征、较高的X射线衰减性能以及肿瘤中优先累积特性[124]。在CT成像中，反应器成像性能显著高于只有TaO_x或Au的单金属系统以及临床使用的碘海醇造影剂技术。生物体外肿瘤CT实验表明：TaO_x@DMSNs-MPTMS-Au不仅出现在肿瘤部分，而且渗透进入肿瘤组织内部。如图6b所示，Li等先将UCNPs用亚甲基蓝(MB)和二氧化硅杂化层包覆，所得UCNPs@(SiO_2&MB)生长树枝状二氧化硅外壳后在其孔道负载溶菌酶(LYZ)[125]。终产物材料UCNPs@(SiO_2&MB)@DMSNs-LYZ经过层层自组装透明质酸(HA)和多聚赖氨酸(PLL)，形成了NIR驱动的PDT杀菌纳米反应器。HA和PLL复合层能够智能控制释放LYZ，反应器在PDT过程产生$^1O_2$，能够强烈杀死病原细菌。

3.1.4 耐摩擦材料 常州大学陈爱莲教授团队制备了SiO_2@DMSNs和SiO_2@MSNs两类核壳状纳米粒子，将其用于化学机械抛光（CMP）研究[126]。DMSNs和MSNs外壳厚度分别为78 ± 3和72 ± 4 nm，孔径分别为3.4和5.0 nm。与传统相同粒径SiO_2粒子相比，SiO_2@DMSNs和SiO_2@MSNs混合研磨剂具有更低的表面形态差异，均方根（RMS）粗糙度分别为0.279和0.408 nm，远低于传统粒子对应的性质（RMS=0.738 nm）。此外，SiO_2@DMSNs的材料去除率（MRR）高于SiO_2@MSNs，得益于前者壳层具有较大接触面积。该课题还考察了DMSNs合成母液中的油相（1-十八烯、萘烷和正己烷）改变对SiO_2@DMSNs形貌结构和CMP性能影响[127]。三种油相成分（C_{18}→C_{10}→C_6）构筑所得SiO_2@DMSNs的比表面为208.1、123.6和141.1 m^2/g；孔体积分别为0.21、0.29和0.27 m^3/g；孔径分布处于3.3、3.6&8.4&11.5和3.6&8.5&11.5 nm。RMS值分别为0.51 ± 0.08、0.39 ± 0.03和0.62 ± 0.05 nm；MRR值分别为271、155和170 nm/min。上述团队以聚苯乙烯（PS）为中心核，合成了核壳结构PS@DMSNs[128]。通过改变DMSNs合成母液中的油相（1-十八烯、萘烷和正己烷）、TEOS添加量及搅拌速率，控制DMSNs壳厚（及孔径）在34 ± 3 ~ 39 ± 4 nm（3.4 ± 0.3 ~ 8.2 ± 0.6 nm）范围变动。空白表面、十八烯和正己烷油相对应PS@DMSNs的RMS值分别为1.39、0.16和0.26 nm。C_{18}和C_6对应PS@DMSNs的MRR值分别为106和72 nm/min。

3.2 树枝状结构为中心核

以DMSNs为载体平台，少量介质负载于其孔道则形成复合结构。随着介质含量增加，DMSNs孔道被完全填充。继续增加介质含量，DMSNs球体会被介质包裹，形成以DMSNs为中心核、介质为壳层的核壳纳米结构。本团队曾研究在DMSNs表面吸附TBOT前驱体并高温煅烧，用以制备硅钛杂化DMSNs-TiO_2复合纳米球[129]。随着TBOT含量增加，DMSNs结构形貌变化如图6c所示，图$6c_5$对应以DMSNs为中心核、TiO_2为壳层的核壳结构。

3.2.1 化学吸附 如图6d所示，Yu等将大量RF填充于DMSNs孔道（图$6d_2$）后，过量RF覆盖纳米球表面（图$6d_3$）[130]。构得DMSNs-RF@RF再次包裹SiO_2层后，经过高温碳化和刻蚀处理，形成具有多级孔结构的纳米碳球（图$6d_4$）。核壳结构DMSNs-RF@RF以及DMSNs-RF@RF@SiO_2为目标设计材料DMSNs-void@C的过渡形态。DMSNs-void@C吸附腐殖酸的最佳饱和吸附量为100 mg/g，吸附遵循准二级动力学方程和Langmuir等温线模型。Zhang等制备的DMSNs@ZIF-8对四环素的饱和吸附容量为751.46 mg/g（ZIF-8仅为549.80 mg/g），吸附遵循准二级动力学方程和Langmuir等温线模型[131]。

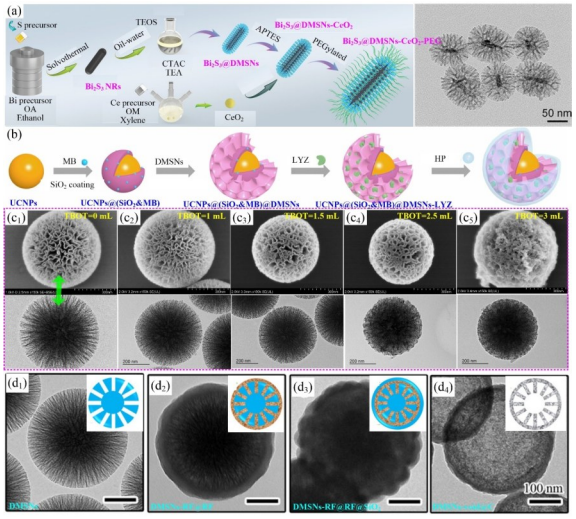

图6 （a）椭球状Bi_2S_3@DMSNs-CeO_2-PEG合成路线及TEM图[117]；（b）纳米反应器UCNPs@(SiO_2&MB)@DMSNs-LYZ@HP的合成过程示意图[125]；（c）本文作者课题组改变TBOT添加量制得系列DMSNs-TiO_2复合物的TEM和SEM图；（d）合成DMSNs-void@C过程涉及纳米粒子的TEM和示意图；包括DMSNs (d_1)；DMSNs-RF@RF (d_2)；DMSNs-RF@RF@SiO_2 (d_3)和DMSNs-void@C (d_4)[130]

Fig.6 (a) Schematic illustration of synthetic procedure for ellipsoidal Bi_2S_3@DMSNs-CeO_2-PEG[117]; (b) Schematic illustration of synthetic route for UCNPs@(SiO_2&MB)@DMSNs-LYZ@HP[125]; (c) TEM and SEM images of various DMSNs-TiO_2 composites in our laboratory by adjusting TBOT dosage from 0 to 3 mL; (d) TEM and inserted illustration images of involved nanoparticles towards DMSNs-void@C; including DMSNs (d_1); DMSNs-RF@RF (d_2); DMSNs-RF@RF@SiO_2 (d_3) and DMSNs-void@C (d_4)[130]

3.2.2 催化合成与降解 如前所述，本团队在制备系列DMSNs-TiO_2过程期望DMSNs负载尽可能多的TiO_2，以此增加反应活性位点数量（图6c）。但同时希望树枝状形貌得以保存，有助于反应介质的迁移和传递。因此，选择图$6c_4$所示DMSNs-TiO_2为理想结构用以吸附和光催化降解染料[129]。Tran等以DMSNs、金纳米点负载的DMSNs-APTES-Au dots和金纳米粒子负载的DMSNs-APTES-AuNPs为中心核，含Zn的金属有机框架（MOF）为壳层，构筑了

DMSNs@MOF 和 DMSNs-APTES-Au@MOF 核壳结构[132]。将上述两类纳米反应器用于催化 Knoevenagel 缩合反应，含金纳米点的 DMSNs-APTES-Au@MOF 底物转化率和循环性能最佳，远高于DMSNs@MOF。

3.2.3 分析检测及分离纯化 Zhang等先将CdTe量子点负载于氨基功能化的DMSNs-APTES孔道，接着使用 APTES 和 MPTMS 混合硅烷对 DMSNs-APTES-CdTe进行固定，最后在复合纳米粒子表面覆盖一层SiO_2[133]。所设计纳米反应器的壳层厚度0 ~ 32 nm范围可控，细胞毒性与壳厚度相关。MTT实验、激光共聚焦扫描显微镜（CLSM）成像、动态细胞摄取及活体荧光成像表明DMSNs-CdTe@SiO_2毒性低、稳定性高且荧光成像性能优越。Huang等构筑了具有显著荧光特性的(DMSNs-MPTMS-QDs)@SiO_2，QDs包括CdSe、CdS或ZnS[134]。将核壳结构依次用APTES和丁二酸酐改性，制得羧基官能团功能化复合结构。基于(DMSNs-QDs)@SiO_2-COOH开发出用于C反应蛋白（CPR）检测的侧流免疫层析诊断技术（LFIA）。通过炔烃和氨的点击化学反应机理，Leng等将炔基修饰的、发射红光的聚集诱导发光材料（AIEgen）接枝于氨基功能化DMSNs-APTES表面，然后覆盖Fe^{3+}-单宁酸（Fe(III)-TA）保护层[135]。抗体在静电作用和配位键合作用下固定于设计构筑的DMSNs-AIEgen@TA表面，形成能增强LFIA的双功能纳米探针反应器。Wu等在金纳米团簇（AuNCs）负载于DMSNs孔道的复合材料（DMSNs-AuNCs）表面覆盖SiO_2保护层，化学接枝APTES后和丁二酸酐反应，制得羧基功能化DMSNs-AuNCs@SiO_2-COOH[136]。配以免疫磁珠，作者建立了快速、灵敏的能够对鼠伤寒沙门氏菌进行检测的荧光免疫分析法，检测限为3 CFU/mL，线性范围为10 ~ 10^6 CFU/mL，对其他食源性病原体不具有选择性。Zhang等制备的DMSNs@ZIF-8作为HPLC固相萃取吸附剂能够高效吸附动物食品中的盐酸四环素。标准曲线线性范围处于20 ~ 500 μg/L，回收率在85.2 ~ 90.7%之间[131]。

4 总结及展望

本综述主要归纳总结了基于树枝状结构的核壳型纳米反应器设计合成及应用研究进展，包括分类、功能化方法及应用领域。该类复合材料基于DMSNs结构特征（即高比表面、大孔体积、较易孔渗透性、颗粒内表面更易接触性、纳米尺度效应等），以应用为导向进行结构设计。主要分为树枝状磁性单一材料核壳型、磁性多样材料核壳型、磁性蛋黄-蛋壳型、非磁性核壳型和非磁性蛋黄-蛋壳型等。这些纳米反应器在化学吸附、催化合成与降解、生物酶固定、分析检测、超湿润界面、药物递送和生物治疗等领域发挥着举足轻重的作用。今后的研究重点及发展前景主要集中在以下三个方面：

4.1 应用导向的材料配置设计

对“树枝状结构的核壳型纳米反应器”而言，分为以下2种基本构成情况，即中心核及树枝状壳层结构，或者树枝状中心核及壳层结构。前者主要发挥树枝状壳层结构与外界环境直接作用（即传质、迁移等）的优势，后者侧重储存于树枝状中心核的活性物质与外界环境的间接接触作用（即隔绝、保护等）。此外，“中心核及树枝状壳层结构”的核芯可选取为磁性和非磁性材料，进而满足磁响应智能需求。以应用导向为设计准则，对中心核及壳层材料进行合理配置是构筑树枝状结构基核壳型纳米反应器的根本策略。本文举出的众多实例均证明上述思路的正确性。

参考本团队在树枝状纳米材料领域的部分基础研究[68, 129, 137-138]，提供一些设计思考与读者共享。例如，磁性核在很多化学反应溶液中易被刻蚀破坏，进而影响纳米反应器的磁响应性能。将M@barrier@DMSNs中的barrier层由现在通用的不耐碱SiO_2替换为性能更加强劲的TiO_2、氮化碳（g-C_3N_4）、聚多巴胺（PDA）等，其对磁性核的保护效用如何？特别是TiO_2和g-C_3N_4，除保护作用外，能否增强催化型纳米反应器的催化性能？再例如，将DMSNs@NM模型中的NM层由现在已开发的SiO_2、DMSNs、MOF、RF等替换为TiO_2、g-C_3N_4、PDA等，能够增加纳米反应器的功能性和实效性？

4.2 功能化官能团设计合成

在本文列举的众多实例中，DMSNs表面硅羟基通常接枝有机硅烷分子实现功能化（图2f,3a）。值得注意的是，虽然商业化硅烷多种多样，但有时难以满足要求。一方面，研究人员可以通过有机合成反应将所需官能团引入硅烷，从而合成新型有机硅烷分子与DMSNs进行“桥梁”（如图3b,c）。另一方面，也可以使用其它能与硅羟基反应的活性基团，如含三元环氧基团的有机分子[139]。由此可知，只要

应用领域确定，便可通过有机合成化学思想进行官能团设计和功能载入。

4.3 结构设计合成

除图1d所示常用树枝状结构的核壳型纳米反应器结构外，其他新颖结构有待开发，以期达到意想不到的材料性能。例如，基于Yang等制备的双壳层空心结构DMSNs[140]，能否将磁性核引入粒子中心来设计构筑具有双壳层结构的磁性核壳状纳米反应器？依此拓展，可在已经出现的特异形貌结构基础上进行创制，如双面神状（Janus）[141]以及羽毛球状[76]DMSNs等。

此外，以应用为导向选定基本结构、材料配置和功能化官能团后，可对各部分组成进行形貌调整，进而探究更加详细的构效关系。例如，磁性材料M可为除球形外的椭球形、纳米链、纳米片等特殊结构（图2a-c），其对纳米反应器磁响应性能影响如何？DMSNs的孔径大小变化（图1c），如何影响化学物质尺寸的选择性和传递速率？DMSNs壳层厚度变化如何影响传质途径和效率？诸如此类设计构筑思路，定将为纳米反应器带来全新性能，亟需投入大量基础研究工作。

参考文献

[1] Kalambate P K, Dhanjai, Huang Z, et al. Core@shell nanomaterials based sensing devices: A review[J]. TrAC Trends in Analytical Chemistry, 2019, **115**: 147-161.
Kalambate P K, Dhanjai, Huang Z M, et al. Core@shell nanomaterials based sensing devices: a review[J]. TrAC Trends in Analytical Chemistry, 2019, **115**: 147-161.[LinkOut]

[2] Gawande M B, Goswami A, Asefa T, et al. Core - shell nanoparticles: synthesis and applications in catalysis and electrocatalysis[J]. Chemical Society Reviews, 2015, **44**(21): 7540-7590.
Gawande M B, Goswami A, Asefa T, et al. Core-shell nanoparticles: synthesis and applications in catalysis and electrocatalysis[J]. Chemical Society Reviews, 2015, **44**(21): 7540-7590.[LinkOut]

[3] Ghosh Chaudhuri R, Paria S, Core/Shell Nanoparticles: Classes, Properties, Synthesis Mechanisms, Characterization, and Applications[J]. Chemical Reviews, 2012, **112**(4): 2373-2433.
Ghosh Chaudhuri R, Paria S. Core/shell nanoparticles: classes, properties, synthesis mechanisms, characterization, and applications[J]. Chemical Reviews, 2012, **112**(4): 2373-2433.[LinkOut]

[4] Zou Y, Sun Z, Wang Q, et al. Core - Shell Magnetic Particles: Tailored Synthesis and Applications[J]. Chemical Reviews, 2025, **125**(2): 972-1048.
Zou Y D, Sun Z K, Wang Q Y, et al. Core-shell magnetic particles: tailored synthesis and applications[J]. Chemical Reviews, 2025, **125**(2): 972-1048.[LinkOut]

[5] Yue Q, Sun J, Kang Y, et al. Advances in the interfacial assembly of mesoporous silica on magnetic particles. Angewandte Chemie International Edition, 2020, **59**(36): 15804 - 15817.
Yue Q, Sun J G, Kang Y J, et al. Advances in the interfacial assembly of mesoporous silica on magnetite particles[J]. Angewandte Chemie International Edition, 2020, **59**(37): 15804-15817.[LinkOut]

[6] Shafiee A, Rabiee N, Ahmadi S, et al. Core - Shell Nanophotocatalysts: Review of Materials and Applications. ACS Applied Nano Materials, 2022, **5**(1): 55 - 86.
Shafiee A, Rabiee N, Ahmadi S, et al. Core-shell nanophotocatalysts: review of materials and applications[J]. ACS Applied Nano Materials, 2022, **5**(1): 55-86.[LinkOut]

[7] Newkome G R, Moorefield C N, Vögtle F. Dendrimers and Dendrons: Concepts, Syntheses, Applications[M]. In Dendrimers and Dendrons, Wiley-VCH Verlag GmbH & Co. KGaA, 2001: pp 1-118.
Newkome G R, Moorefield C N, Vögtle F. Dendrimers and Dendrons: Concepts, Syntheses, Applications[M]. Wiley, 2001.[LinkOut]

[8] Fréchet J M J, Tomalia D A. Dendrimers and Other Dendritic Polymers[M]. John Wiley & Sons, 2002: 3-40.
Fréchet J M J, Tomalia D A. Dendrimers and Other Dendritic Polymers[M]. Wiley, 2001.[LinkOut]

[9] Polshettiwar V, Cha D, Zhang X, et al. High-surface-area silica nanospheres (KCC-1) with a fibrous morphology[J]. Angewandte Chemie International Edition, 2010, **49**(50): 9652-9656.
Polshettiwar V, Cha D, Zhang X X, et al. High-surface-area silica nanospheres (KCC-1) with a fibrous morphology[J]. Angewandte Chemie International Edition, 2010, **49**(50): 9652-9656.[LinkOut]

[10] Xu C, Lei C, Wang Y, et al. Dendritic mesoporous nanoparticles: Structure, synthesis and properties[J]. Angewandte Chemie International Edition, 2022, **61**: e202112752.
Xu C, Lei C, Wang Y, et al. Dendritic mesoporous nanoparticles: structure, synthesis and properties[J]. Angewandte Chemie International Edition, 2022, **61**(12): e202112752.[LinkOut]

[11] Wang Y, Du X, Liu Z, et al. Dendritic fibrous nano-particles (DFNPs): Rising stars of mesoporous materials[J]. Journal of Materials Chemistry A, 2019, **7**(10): 5111-5152.
Wang Y B, Du X, Liu Z, et al. Dendritic fibrous nano-particles (DFNPs): rising stars of mesoporous materials[J]. Journal of Materials Chemistry A, 2019, **7**(10): 5111-5152.[LinkOut]

[12] Wang Y, Zhang B, Ding X, et al. Dendritic mesoporous organosilica nanoparticles (DMONs): Chemical composition, structural architecture, and promising applications[J]. Nano Today, 2021, **39**: 101231.
Wang Y B, Zhang B L, Ding X P, et al. Dendritic mesoporous organosilica nanoparticles (DMONs): chemical composition, structural architecture, and promising applications[J]. Nano Today, 2021, **39**: 101231.[LinkOut]

[13] Wang Y, Huang L, Li S, et al. The capture and catalytic conversion of CO_2 by dendritic mesoporous silica-based nanoparticles[J]. Energy & Environmental Materials, 2024, **7**(2): e12593.
Wang Y B, Huang L Z, Li S W, et al. The capture and catalytic conversion of CO_2 by dendritic mesoporous silica-based

nanoparticles[J]. Energy & Environmental Materials, 2024, **7**(2): e12593.[LinkOut]

[14] Maity A, Belgamwar R, Polshettiwar V. Facile synthesis to tune size, textural properties and fiber density of dendritic fibrous nanosilica for applications in catalysis and CO_2 capture[J]. Nature protocols, 2019, **14**: 2177 – 2204.
Maity A, Belgamwar R, Polshettiwar V. Facile synthesis to tune size, textural properties and fiber density of dendritic fibrous nanosilica for applications in catalysis and CO_2 capture[J]. Nature Protocols, 2019, **14**(7): 2177–2204.[LinkOut]

[15] Wang Z, Brown A T, Tan K, et al. Selective Extraction of Thorium from Rare Earth Elements Using Wrinkled Mesoporous Carbon[J]. Journal of the American Chemical Society, 2018, **140**: 14735–14739.
Wang Z J, Brown A T, Tan K, et al. Selective extraction of thorium from rare earth elements using wrinkled mesoporous carbon[J]. Journal of the American Chemical Society, 2018, **140**(44): 14735–14739.[LinkOut]

[16] Shao D, Li M, Wang Z, et al. Bioinspired Diselenide–Bridged Mesoporous Silica Nanoparticles for Dual–Responsive Protein Delivery[J]. Advanced Materials, 2018, **30**(29): 1801198.
Shao D, Li M Q, Wang Z, et al. Bioinspired diselenide–bridged mesoporous silica nanoparticles for dual–responsive protein delivery[J]. Advanced Materials, 2018, **30**(29): 1801198.[LinkOut]

[17] Yue Q, Li J, Luo W, et al. An Interface coassembly in biliquid phase: toward core–shell magnetic mesoporous silica microspheres with tunable pore size[J]. Journal of the American Chemical Society, 2015, **137**(41): 13282–13289.
Yue Q, Li J L, Luo W, et al. An interface coassembly in biliquid phase: toward core–shell magnetic mesoporous silica microspheres with tunable pore size[J]. Journal of the American Chemical Society, 2015, **137**(41): 13282–13289.[LinkOut]

[18] Abbaraju P L, Meka A K, Song H, et al. Asymmetric silica nanoparticles with tunable head – tail structures enhance hemocompatibility and maturation of immune cells[J]. Journal of the American Chemical Society, 2017, **139**(18): 6321–6328.
Abbaraju P L, Meka A K, Song H, et al. Asymmetric silica nanoparticles with tunable head–tail structures enhance hemocompatibility and maturation of immune cells[J]. Journal of the American Chemical Society, 2017, **139**(18): 6321–6328.[LinkOut]

[19] Xing Y, Pan Q, Du X, et al. Dendritic Janus Nanomotors with Precisely Modulated Coverages and Their Effects on Propulsion [J]. ACS Applied Materials & Interfaces, 2019, **11**(10): 10426–10433.
Xing Y, Pan Q, Du X, et al. Dendritic Janus nanomotors with precisely modulated coverages and their effects on propulsion[J]. ACS Applied Materials & Interfaces, 2019, **11**(10): 10426–10433.[LinkOut]

[20] Bayal N, Singh B, Singh R, et al. Size and Fiber Density Controlled Synthesis of Fibrous Nanosilica Spheres (KCC–1) [J]. Scientific Reports, 2016, **6**: 24888.
Bayal N, Singh B, Singh R, et al. Size and fiber density controlled synthesis of fibrous nanosilica spheres (KCC–1) [J]. Scientific Reports, 2016, **6**: 24888.[LinkOut]

[21] Yu K, Zhang X, Tong H, et al. Synthesis of fibrous monodisperse core – shell Fe_3O_4/SiO_2/KCC–1[J]. Materials Letters, 2013, **106** (9): 151–154.
Yu K J, Zhang X B, Tong H W, et al. Synthesis of fibrous monodisperse core–shell Fe_3O_4/SiO_2/KCC–1[J]. Materials Letters, 2013, **106**: 151–154.[LinkOut]

[22] Nemec S, Kralj S. A versatile interfacial coassembly method for fabrication of tunable silica shells with radially aligned dual mesopores on diverse magnetic core nanoparticles[J]. ACS Applied Materials & Interfaces, 2021, **13**(1): 1883–1894.
Nemec S, Kralj S. A versatile interfacial coassembly method for fabrication of tunable silica shells with radially aligned dual mesopores on diverse magnetic core nanoparticles[J]. ACS Applied Materials & Interfaces, 2021, **13**(1): 1883–1894.[LinkOut]

[23] Emrani S, Ebrahimi M, Zhiani R, et al. Magnetic fibrous silica mesoporous as a selective and efficient system for removal of Cd (II) ions with a focus on optimization by response surface methodology[J]. International Journal of Environmental Analytical Chemistry, 2021, **103**(4): 849 – 867.
Emrani S, Ebrahimi M, Zhiani R, et al. Magnetic fibrous silica mesoporous as a selective and efficient system for removal of Cd (II) ions with a focus on optimization by response surface methodology[J]. International Journal of Environmental Analytical Chemistry, 2023, **103**(4): 849–867.[LinkOut]

[24] Salari Goharrizi F, Ebrahimipour S Y, Ebrahimnejad H, et al. Novel magnetic adsorbents based on mesoporous KCC–1 for the removal of heavy metal ions and antibacterial applications[J]. Journal of Inorganic and Organometallic Polymers and Materials, 2024, **34**(11): 5425–5441.
Salari Goharrizi F, Ebrahimipour S Y, Ebrahimnejad H, et al. Novel magnetic adsorbents based on mesoporous KCC–1 for the removal of heavy metal ions and antibacterial applications[J]. Journal of Inorganic and Organometallic Polymers and Materials, 2024, **34**(11): 5425–5441.[LinkOut]

[25] Goharrizi F S, Ebrahimipour S Y, Ebrahimnejad H, et al. Magnetic mesoporous silica functionalized with amine groups for efficient removal of heavy metals and bacterial inhibition[J]. Journal of Cluster Science, 2024, **35**(7): 2419–2435.
Goharrizi F S, Ebrahimipour S Y, Ebrahimnejad H, et al. Magnetic mesoporous silica functionalized with amine groups for efficient removal of heavy metals and bacterial inhibition[J]. Journal of Cluster Science, 2024, **35**(7): 2419–2435.[LinkOut]

[26] Wang F, Li T, Liao Y, et al. The synthesis of core–shell magnetic dendritic fibrous nano–silica for the fast and selective capture of U (VI) [J]. Applied Surface Science, 2023, **638**: 157969.
Wang F, Li T T, Liao Y, et al. The synthesis of core–shell magnetic dendritic fibrous nano–silica for the fast and selective capture of U(VI)[J]. Applied Surface Science, 2023, **638**: 157969.[LinkOut]

[27] Wang F, Chen Z, Wu Y, et al. The amidoxime–functionalized magnetic dendritic fibrous nano–silica with a core – shell structure for the efficient capture of U(VI) [J]. Applied Surface Science, 2025, **680**: 161491.
Wang F, Chen Z, Wu Y, et al. The amidoxime–functionalized magnetic dendritic fibrous nano–silica with a core–shell structure for the efficient capture of U(VI) [J]. Applied Surface Science, 2025, **680**: 161491.[LinkOut]

[28] Lyu J, Zhang F, Li R, et al. Magnetic core supported ethyl acetate

microdrops for organic contaminants removal from water[J]. npj Clean Water, 2024, **7**(1): 96.
Lyu J, Zhang F M, Li R, et al. Magnetic core supported ethyl acetate microdrops for organic contaminants removal from water [J]. npj Clean Water, 2024, **7**: 96.[LinkOut]

[29] Zhang W, Li S, Zhang J, et al. Synthesis and adsorption behavior study of magnetic fibrous mesoporous silica[J]. Microporous and Mesoporous Materials, 2019, **282**: 15-21.
Zhang W, Li S M, Zhang J, et al. Synthesis and adsorption behavior study of magnetic fibrous mesoporous silica[J]. Microporous and Mesoporous Materials, 2019, **282**: 15-21. [LinkOut]

[30] Yang J, Shen D, Wei Y, et al. Monodisperse core-shell structured magnetic mesoporous aluminosilicate nanospheres with large dendritic mesochannels[J]. Nano Research, 2015, **8**(8): 2503-2514.
Yang J P, Shen D K, Wei Y, et al. Monodisperse core-shell structured magnetic mesoporous aluminosilicate nanospheres with large dendritic mesochannels[J]. Nano Research, 2015, **8**(8): 2503-2514.[LinkOut]

[31] Gao J, Kong W, Zhou L, et al. Monodisperse core-shell magnetic organosilica nanoflowers with radial wrinkle for lipase immobilization[J]. Chemical Engineering Journal, 2017, **309**: 70-79.
Gao J, Kong W X, Zhou L Y, et al. Monodisperse core-shell magnetic organosilica nanoflowers with radial wrinkle for lipase immobilization[J]. Chemical Engineering Journal, 2017, **309**: 70-79.[LinkOut]

[32] Goharrizi F S, Ebrahimipour S Y, Mahani M T, et al. Enhanced stability and activity of diaphorase enzyme immobilized on magnetic mesoporous silica[J]. Journal of Porous Materials, 2025, **32**(4): 1607-1625.
Goharrizi F S, Ebrahimipour S Y, Mahani M T, et al. Enhanced stability and activity of diaphorase enzyme immobilized on magnetic mesoporous silica[J]. Journal of Porous Materials, 2025, **32**(4): 1607-1625.[LinkOut]

[33] Ali Z, Tian L, Zhang B, et al. Synthesis of paramagnetic dendritic silica nanomaterials with fibrous pore structure (Fe_3O_4@KCC-1) and their application in immobilization of lipase from Candida rugosa with enhanced catalytic activity and stability[J]. New Journal of Chemistry, 2017, **41**(16): 8222-8231.
Ali Z, Tian L, Zhang B L, et al. Synthesis of paramagnetic dendritic silica nanomaterials with fibrous pore structure (Fe_3O_4@KCC-1) and their application in immobilization of lipase from *Candida rugosa* with enhanced catalytic activity and stability [J]. New Journal of Chemistry, 2017, **41**(16): 8222-8231.[LinkOut]

[34] Liu D, Wang X, Jiang Y. Design of enzyme nanoreactor by phase-transitioned lysozyme modified magnetic dendritic silica nanoparticle for efficient catalytic performance at harsh reaction condition[J]. Materials Science and Engineering: B, 2023, **292**: 116442.
Liu D Q, Wang X, Jiang Y C. Design of enzyme nanoreactor by phase-transitioned lysozyme modified magnetic dendritic silica nanoparticle for efficient catalytic performance at harsh reaction condition[J]. Materials Science and Engineering: B, 2023, **292**: 116442.[LinkOut]

[35] Asghari E, Saraji M. Preparation of a magnetic molecularly imprinted polymer on fibrous silica nanosphere via self-polycondensation for micro solid-phase extraction of chlorpyrifos [J]. Journal of Chromatography B, 2024, **1232**: 123961.
Asghari E, Saraji M. Preparation of a magnetic molecularly imprinted polymer on fibrous silica nanosphere *via* self-polycondensation for micro solid-phase extraction of chlorpyrifos [J]. Journal of Chromatography B, 2024, **1232**: 123961.[LinkOut]

[36] Sun Z, Li H, Guo D, et al. A multifunctional magnetic core-shell fibrous silica sensing probe for highly sensitive detection and removal of Zn^{2+} from aqueous solution[J]. Journal of Materials Chemistry C, 2015, **3**(18): 4713-4722.
Sun Z B, Li H Z, Guo D, et al. A multifunctional magnetic core-shell fibrous silica sensing probe for highly sensitive detection and removal of Zn^{2+} from aqueous solution[J]. Journal of Materials Chemistry C, 2015, **3**(18): 4713-4722.[LinkOut]

[37] Radhakrishnan K, Panneerselvam P, Ravikumar A. A hybrid magnetic core-shell fibrous silica nanocomposite for a chemosensor-based highly effective fluorescent detection of Cu(II) [J]. RSC Advances, 2017, **7**(72): 45824-45833.
Radhakrishnan K, Panneerselvam P, Ravikumar A. A hybrid magnetic core-shell fibrous silica nanocomposite for a chemosensor-based highly effective fluorescent detection of Cu(II) [J]. RSC Advances, 2017, **7**(72): 45824-45833.[LinkOut]

[38] Radhakrishnan K, Panneerselvam P, Ravikumar A, et al. Magnetic core-shell fibrous silica functionalized with pyrene derivative for highly sensitive and selective detection of Hg (II) ion [J]. Journal of Dispersion Science and Technology, 2019, **40**(9): 1368-1377.
Radhakrishnan K, Panneerselvam P, Ravikumar A, et al. Magnetic core-shell fibrous silica functionalized with pyrene derivative for highly sensitive and selective detection of Hg (II) ion [J]. Journal of Dispersion Science and Technology, 2019, **40**(9): 1368-1377.[LinkOut]

[39] Zhao X, Dong J, Zhang Y, et al. Magnetic dendritic mesoporous silica nanoparticles based integrated platform for rapid and efficient analysis of saccharides[J]. Analytica Chimica Acta, 2024, **1288**: 342166.
Zhao X L, Dong J C, Zhang Y Q, et al. Magnetic dendritic mesoporous silica nanoparticles based integrated platform for rapid and efficient analysis of saccharides[J]. Analytica Chimica Acta, 2024, **1288**: 342166.[LinkOut]

[40] Cao G, Gao J, Zhou L, et al. Fabrication of Ni^{2+}-nitrilotriacetic acid functionalized magnetic mesoporous silica nanoflowers for one pot purification and immobilization of His-tagged ω-transaminase[J]. Biochemical Engineering Journal, 2017, **128**: 116-125.
Cao G X, Gao J, Zhou L Y, et al. Fabrication of Ni^{2+}-nitrilotriacetic acid functionalized magnetic mesoporous silica nanoflowers for one pot purification and immobilization of His-tagged *ω* -transaminase[J]. Biochemical Engineering Journal, 2017, **128**: 116-125.[LinkOut]

[41] Hong Y, Zhan Q, Zheng Y, et al., Hydrophilic phytic acid-functionalized magnetic dendritic mesoporous silica nanospheres with immobilized Ti^{4+}: A dual-purpose affinity material for highly efficient enrichment of glycopeptides/phosphopeptides[J]. Talanta, 2019, **197**: 77-85.
Hong Y Y, Zhan Q L, Zheng Y, et al. Hydrophilic phytic acid-

functionalized magnetic dendritic mesoporous silica nanospheres with immobilized Ti^{4+}: a dual-purpose affinity material for highly efficient enrichment of glycopeptides/phosphopeptides[J]. Talanta, 2019, **197**: 77-85.[LinkOut]

[42] Jin P, Zhu F, Zhou W, et al. Developing magnetic functionalized dendritic fibrous mesoporous silica as advanced adsorbent for quaternary ammonium alkaloids[J]. Microchimica Acta, 2023, **190** (12): 481.
Jin P, Zhu F C, Zhou W, et al. Developing magnetic functionalized dendritic fibrous mesoporous silica as advanced adsorbent for quaternary ammonium alkaloids[J]. Microchimica Acta, 2023, **190** (12): 481.[LinkOut]

[43] Dong Z, Yu G, Le X. Gold nanoparticle modified magnetic fibrous silica microspheres as a highly efficient and recyclable catalyst for the reduction of 4-nitrophenol[J]. New Journal of Chemistry, 2015, **39**(11): 8623-8629.
Dong Z P, Yu G Q, Le X. Gold nanoparticle modified magnetic fibrous silica microspheres as a highly efficient and recyclable catalyst for the reduction of 4-nitrophenol[J]. New Journal of Chemistry, 2015, **39**(11): 8623-8629.[LinkOut]

[44] Sun Z, Li H, Cui G, et al. Multifunctional magnetic core - shell dendritic mesoporous silica nanospheres decorated with tiny Ag nanoparticles as a highly active heterogeneous catalyst[J]. Applied Surface Science, 2016, **360**: 252-262.
Sun Z B, Li H Z, Cui G J, et al. Multifunctional magnetic core-shell dendritic mesoporous silica nanospheres decorated with tiny Ag nanoparticles as a highly active heterogeneous catalyst[J]. Applied Surface Science, 2016, **360**: 252-262.[LinkOut]

[45] Sadeghzadeh S. M. A green approach for the synthesis of 2-oxazolidinones using gold(I) complex immobilized on KCC-1 as nanocatalyst at room temperature[J]. Applied Organometallic Chemistry, 2016, **30**(10): 835-842.
Sadeghzadeh S M. A green approach for the synthesis of 2-oxazolidinones using gold(I) complex immobilized on KCC-1 as nanocatalyst at room temperature[J]. Applied Organometallic Chemistry, 2016, **30**(10): 835-842.[LinkOut]

[46] Sadeghzadeh S M. A heteropolyacid-based ionic liquid immobilized onto magnetic fibrous nano-silica as robust and recyclable heterogeneous catalysts for the synthesis of tetrahydrodipyrazolopyridines in water[J]. RSC Advances, 2016, **6** (79): 75973-75980.
Sadeghzadeh S M. A heteropolyacid-based ionic liquid immobilized onto magnetic fibrous nano-silica as robust and recyclable heterogeneous catalysts for the synthesis of tetrahydrodipyrazolopyridines in water[J]. RSC Advances, 2016, **6** (79): 75973-75980.[LinkOut]

[47] Sadeghzadeh S M. Bis(4-pyridylamino)triazine-stabilized magnetite KCC-1: a chemoselective, efficient, green and reusable nanocatalyst for the synthesis of N-substituted 1, 4-dihydropyridines[J]. RSC Advances, 2016, **6**(101): 99586-99594.
Sadeghzadeh S M. Bis(4-pyridylamino)triazine-stabilized magnetite KCC-1: a chemoselective, efficient, green and reusable nanocatalyst for the synthesis of N-substituted 1, 4-dihydropyridines[J]. RSC Advances, 2016, **6**(101): 99586-99594.[LinkOut]

[48] Zhao Y, Tang J J, Motavalizadehkakhky A, et al. Synthesis and characterization of a novel CNT-FeNi3/DFNS/Cu(ii) magnetic nanocomposite for the photocatalytic degradation of tetracycline in wastewater[J]. RSC Advances, 2019, **9**(60): 35022-35032.
Zhao Y H, Tang J J, Motavalizadehkakhky A, et al. Synthesis and characterization of a novel CNT-$FeNi_3$/DFNS/Cu(II) magnetic nanocomposite for the photocatalytic degradation of tetracycline in wastewater[J]. RSC Advances, 2019, **9**(60): 35022-35032.[LinkOut]

[49] Hassankhani A, Sadeghzadeh S M, Zhiani R. C-C and C-H coupling reactions by Fe_3O_4/KCC-1/APTPOSS supported palladium-salen-bridged ionic networks as a reusable catalyst[J]. RSC Advances, 2018, **8**(16): 8761-8769.
Hassankhani A, Sadeghzadeh S M, Zhiani R. C-C and C-H coupling reactions by Fe_3O_4/KCC-1/APTPOSS supported palladium-salen-bridged ionic networks as a reusable catalyst[J]. RSC Advances, 2018, **8**(16): 8761-8769.[LinkOut]

[50] Saadati S M, Zhiani R, Zahedifar M, et al. Synthesis of tetramethylquinoline-2, 4-diamine using FeNi3/KCC-1/APTPOSS-supported copper cyclam and salen complex as a reusable catalyst[J]. Applied Organometallic Chemistry, 2018, **32** (12): e4560.
Saadati S M, Zhiani R, Zahedifar M, et al. Synthesis of tetramethylquinoline-2, 4-diamine using $FeNi_3$/KCC-1/APTPOSS-supported copper cyclam and salen complex as a reusable catalyst[J]. Applied Organometallic Chemistry, 2018, **32** (12): e4560.[LinkOut]

[51] Qiu J, Yu L, Ni J. et al. Palladium - salen-bridged ionic networks immobilized on magnetic dendritic silica fibers for the synthesis of cyclic carbonates by oxidative carboxylation[J]. New Journal of Chemistry, 2020, **44**(4): 1269-1277.
Qiu J P, Yu L, Ni J G, et al. Palladium-salen-bridged ionic networks immobilized on magnetic dendritic silica fibers for the synthesis of cyclic carbonates by oxidative carboxylation[J]. New Journal of Chemistry, 2020, **44**(4): 1269-1277.[LinkOut]

[52] Fei Z Chen F, Zhong M, et al. Synthesis and characterization of a novel ruthenium(ii) trisbipyridine complex magnetic nanocomposite for the selective oxidation of phenols[J]. RSC Advances, 2019, **9**(48): 28078-28088.
Fei Z X, Chen F, Zhong M Q, et al. Synthesis and characterization of a novel ruthenium(II) trisbipyridine complex magnetic nanocomposite for the selective oxidation of phenols[J]. RSC Advances, 2019, **9**(48): 28078-28088.[PubMed]

[53] Zhiani R, Es-haghi A, Saadati S M, et al. A new class of organocobaloximes based FeNi3/DFNS for reduction of 4-nitrophenol and 2-nitroaniline[J]. Journal of Organometallic Chemistry, 2018, **877**: 21-31.
Zhiani R, Es-haghi A, Saadati S M, et al. A new class of organocobaloximes based $FeNi_3$/DFNS for reduction of 4-nitrophenol and 2-nitroaniline[J]. Journal of Organometallic Chemistry, 2018, **877**: 21-31.[LinkOut]

[54] Zhang Q, Wu Y, Wang M, et al. Synthesis and photocatalytic performance of recyclable core-shell mesoporous Fe_3O_4@Bi_2WO_6 nanoparticles. Materials Research Bulletin, 2019, 113: 223-230.
Zhang Q, Wu Y H, Wang M Z, et al. Synthesis and photocatalytic performance of recyclable core-shell mesoporous Fe_3O_4@Bi_2WO_6 nanoparticles[J]. Materials Research Bulletin, 2019, **113**: 223-230.[LinkOut]

[55] Zhiani R, Khoobi M, Sadeghzadeh S M, Synthesis of N- [(2-

hydroxyethoxy)carbonyl]glycine from carbon dioxide, ethylene oxide, and α -amino acid by ionic gelation of sodium tripolyphosphate (TPP) and spirulina supported on magnetic KCC-1 in aqueous solution[J]. New Journal of Chemistry, 2018, **42**(12): 10153-10160.

Zhiani R, Khoobi M, Sadeghzadeh S M. Synthesis of *N*- [(2-hydroxyethoxy)carbonyl] glycine from carbon dioxide, ethylene oxide, and α -amino acid by ionic gelation of sodium tripolyphosphate (TPP) and spirulina supported on magnetic KCC-1 in aqueous solution[J]. New Journal of Chemistry, 2018, **42**(12): 10153-10160.[LinkOut]

[56] Asadi Zeydabadi H, Mehrzad J, Motavalizadehkakhky A, et al. Fixing CO_2 into β -Oxopropylcarbamatesin by Palladium NPs Supported on Magnetic Fibrous Silica Ionic Gelation[J]. Catalysis Letters, 2021, **151**(2): 582-592.

Asadi Zeydabadi H, Mehrzad J, Motavalizadehkakhky A, et al. Fixing CO_2 into β -oxopropylcarbamatesin by palladium NPs supported on magnetic fibrous silica ionic gelation[J]. Catalysis Letters, 2021, **151**(2): 582-592.[LinkOut]

[57] Hasanpour Galehban M, Zeynizadeh B, Mousavi H. Diverse and efficient catalytic applications of new cockscomb flower-like Fe_3O_4@SiO_2@KCC-1@MPTMS@CuII mesoporous nanocomposite in the environmentally benign reduction and reductive acetylation of nitroarenes and one-pot synthesis of some coumarin compounds [J]. RSC Advances, 2022, **12**(18): 11164-11189.

Hasanpour Galehban M, Zeynizadeh B, Mousavi H. Diverse and efficient catalytic applications of new cockscomb flower-like Fe_3O_4@SiO_2@KCC-1@MPTMS@Cu^{II} mesoporous nanocomposite in the environmentally benign reduction and reductive acetylation of nitroarenes and one-pot synthesis of some coumarin compounds [J]. RSC Advances, 2022, **12**(18): 11164-11189.[LinkOut]

[58] Galehban M H, Zeynizadeh B, Mousavi H. Introducing Fe_3O_4@SiO_2@KCC-1@MPTMS@CuII catalytic applications for the green one-pot syntheses of 2-aryl (or heteroaryl) -2, 3-dihydroquinazolin-4(1H)-ones and 9-aryl-3,3,6,6-tetramethyl-3,4,5,6,7,9-hexahydro-1H-xanthene-1,8(2H)-diones[J]. Journal of Molecular Structure, 2023, **1271**: 134017.

Galehban M H, Zeynizadeh B, Mousavi H. Introducing Fe_3O_4@SiO_2@KCC-1@MPTMS@Cu^{II} catalytic applications for the green one-pot syntheses of 2-aryl(or heteroaryl) -2, 3-dihydroquinazolin-4(1*H*)-ones and 9-aryl-3, 3, 6, 6-tetramethyl-3, 4, 5, 6, 7, 9-hexahydro-1*H*-xanthene-1, 8(2*H*) -diones[J]. Journal of Molecular Structure, 2023, **1271**: 134017.[LinkOut]

[59] Saberi S, Zhiani R, Mehrzad J. et al. Synthesis and characterization of a novel TEMPO@FeNi3/DFNS - laccase magnetic nanocomposite for the reduction of nitro compounds[J]. RSC Advances, 2020, **10**(46): 27297-27304.

Saberi S, Zhiani R, Mehrzad J, et al. Synthesis and characterization of a novel TEMPO@$FeNi_3$/DFNS-laccase magnetic nanocomposite for the reduction of nitro compounds[J]. RSC Advances, 2020, **10**(46): 27297-27304.[LinkOut]

[60] Seo B, Lee C, Yoo D, et al. A magnetically recoverable photocatalyst prepared by supporting TiO_2 nanoparticles on a superparamagnetic iron oxide nanocluster core@fibrous silica shell nanocomposite[J]. RSC Advances, 2017, **7**(16): 9587-9595.

Seo B, Lee C, Yoo D, et al. A magnetically recoverable photocatalyst prepared by supporting TiO_2 nanoparticles on a superparamagnetic iron oxide nanocluster core@fibrous silica shell nanocomposite[J]. RSC Advances, 2017, **7**(16): 9587-9595.[LinkOut]

[61] Wei J, Zou L, Li Y, et al. Synthesis of core - shell-structured mesoporous silica nanospheres with dual-pores for biphasic catalysis[J]. New Journal of Chemistry, 2019, **43**(15): 5833-5838.

Wei J, Zou L K, Li Y L, et al. Synthesis of core-shell-structured mesoporous silica nanospheres with dual-pores for biphasic catalysis[J]. New Journal of Chemistry, 2019, **43**(15): 5833-5838.[LinkOut]

[62] Qiu P, Zhao T, Khim J, et al. Ordered mesoporous carbon-silica frameworks confined magnetic mesoporous TiO_2 as an efficient catalyst under acoustic cavitation energy[J]. Journal of Materiomics, 2020, **6**(1): 45-53.

Qiu P P, Zhao T, Khim J, et al. Ordered mesoporous carbon-silica frameworks confined magnetic mesoporous TiO_2 as an efficient catalyst under acoustic cavitation energy[J]. Journal of Materiomics, 2020, **6**(1): 45-53.[LinkOut]

[63] Gu Z, Liu T, Tang J, et al. Mechanism of iron oxide-induced macrophage activation: The impact of composition and the underlying signaling pathway[J]. Journal of the American Chemical Society, 2019, **141**(15): 6122-6126.

Gu Z Y, Liu T Q, Tang J, et al. Mechanism of iron oxide-induced macrophage activation: the impact of composition and the underlying signaling pathway[J]. Journal of the American Chemical Society, 2019, **141**(15): 6122-6126.[PubMed]

[64] Tsh A, Lee J H, Lee J J, et al. Mesoporous silica with fibrous morphology: a multifunctional core-shell platform for biomedical applications[J]. Nanotechnology, 2013, **24**(34): 345603.

Atabaev T S, Lee J H, Lee J J, et al. Mesoporous silica with fibrous morphology: a multifunctional core-shell platform for biomedical applications[J]. Nanotechnology, 2013, **24**(34): 345603.[LinkOut]

[65] Chen J, Lei S, Zeng K, et al. Catalase-imprinted Fe_3O_4/Fe@fibrous SiO_2/polydopamine nanoparticles: An integrated nanoplatform of magnetic targeting, magnetic resonance imaging, and dual-mode cancer therapy[J]. Nano Research, 2017, **10** (7): 2351-2363.

Chen J X, Lei S, Zeng K, et al. Catalase-imprinted Fe_3O_4/Fe@fibrous SiO_2/polydopamine nanoparticles: an integrated nanoplatform of magnetic targeting, magnetic resonance imaging, and dual-mode cancer therapy[J]. Nano Research, 2017, **10**(7): 2351-2363.[LinkOut]

[66] Fiedler R, Sivakumaran G, Mallén J, et al. Superparamagnetic core - mesoporous silica shell nanoparticles with tunable extra- and intracellular dissolution rates[J]. Chemistry of Materials, 2024, **36** (6): 2790-2798.

Fiedler R, Sivakumaran G, Mallén J, et al. Superparamagnetic core-mesoporous silica shell nanoparticles with tunable extra- and intracellular dissolution rates[J]. Chemistry of Materials, 2024, **36**(6): 2790-2798.[LinkOut]

[67] Alamri H, Al-Shahrani A, Bovero E, et al. Self-cleaning superhydrophobic epoxy coating based on fibrous silica-coated iron oxide magnetic nanoparticles[J]. Journal of Colloid and Interface Science, 2018, **513**: 349-356.

Alamri H, Al-Shahrani A, Bovero E, et al. Self-cleaning superhydrophobic epoxy coating based on fibrous silica-coated

iron oxide magnetic nanoparticles[J]. Journal of Colloid and Interface Science, 2018, **513**: 349-356.[LinkOut]

[68] Wang Y, Wu P, Wang Y, et al. Controllable pore size of super-hydrophobic magnetic core-shell nanospheres with dendritic architecture and their pore-dependent performances in oil/water separation[J]. Separation and Purification Technology, 2023, **323**: 124434.
Wang Y B, Wu P, Wang Y N, et al. Controllable pore size of super-hydrophobic magnetic core-shell nanospheres with dendritic architecture and their pore-dependent performances in oil/water separation[J]. Separation and Purification Technology, 2023, **323**: 124434.[LinkOut]

[69] Wang B, Wei Y, Wang Q, et al. Superhydrophobic magnetic core - shell mesoporous organosilica nanoparticles with dendritic architecture for oil - water separation[J]. Materials Chemistry Frontiers, 2020, **4**: 2184-2191
Wang B X, Wei Y Z, Wang Q F, et al. Superhydrophobic magnetic core-shell mesoporous organosilica nanoparticles with dendritic architecture for oil-water separation[J]. Materials Chemistry Frontiers, 2020, **4**(7): 2184-2191.[LinkOut]

[70] Ali Z, Tian L, Zhang B, et al. Synthesis of fibrous and non-fibrous mesoporous silica magnetic yolk - shell microspheres as recyclable supports for immobilization of Candida rugosa lipase[J]. Enzyme and Microbial Technology, 2017, **103**: 42-52.
Ali Z, Tian L, Zhang B L, et al. Synthesis of fibrous and non-fibrous mesoporous silica magnetic yolk-shell microspheres as recyclable supports for immobilization of *Candida rugosa* lipase [J]. Enzyme and Microbial Technology, 2017, **103**: 42-52.[LinkOut]

[71] Bian L, Deng W, Xie D, et al. Dendritic Mesoporous Silica Hollow Spheres with One-Pot Self-Templated Interfacial Diffusion Method[J]. Chemistry of Materials, 2024, **36**(1): 482-491.
Bian L, Deng W J, Xie D, et al. Dendritic mesoporous silica hollow spheres with one-pot self-templated interfacial diffusion method[J]. Chemistry of Materials, 2024, **36**(1): 482-491.[LinkOut]

[72] Yang Y, Bernardi S, Song H, et al. Anion Assisted Synthesis of Large Pore Hollow Dendritic Mesoporous Organosilica Nanoparticles: Understanding the Composition Gradient[J]. Chemistry of Materials, 2016, **28**(3): 704-707.
Yang Y N, Bernardi S, Song H, et al. Anion assisted synthesis of large pore hollow dendritic mesoporous organosilica nanoparticles: understanding the composition gradient[J]. Chemistry of Materials, 2016, **28**(3): 704-707.[LinkOut]

[73] Yang Y, Lu Y, Abbaraju P L, et al. Stepwise Degradable Nanocarriers Enabled Cascade Delivery for Synergistic Cancer Therapy[J]. Advanced Functional Materials, 2018, **28**(28): 1800706.
Yang Y N, Lu Y, Abbaraju P L, et al. Stepwise degradable nanocarriers enabled cascade delivery for synergistic cancer therapy[J]. Advanced Functional Materials, 2018, **28**(28): 1800706.[LinkOut]

[74] Du X, Zhao C, Luan Y, et al. Dendritic porous yolk@ordered mesoporous shell structured heterogeneous nanocatalysts with enhanced stability[J]. Journal of Materials Chemistry A, 2017, **5** (40): 21560-21569.
Du X, Zhao C X, Luan Y, et al. Dendritic porous yolk@ordered mesoporous shell structured heterogeneous nanocatalysts with enhanced stability[J]. Journal of Materials Chemistry A, 2017, **5** (40): 21560-21569.[LinkOut]

[75] Du X, Zhao C, Li X, et al. Novel yolk-shell polymer/carbon@Au nanocomposites by using dendrimer-like mesoporous silica nanoparticles as hard template[J]. Journal of Alloys and Compounds, 2017, **700**: 83-91.
Du X, Zhao C X, Li X Y, et al. Novel yolk-shell polymer/carbon@Au nanocomposites by using dendrimer-like mesoporous silica nanoparticles as hard template[J]. Journal of Alloys and Compounds, 2017, **700**: 83-91.[LinkOut]

[76] Moon D S, Lee J K. Formation of wrinkled silica mesostructures based on the phase behavior of pseudoternary systems[J]. Langmuir, 2014, **30**(51): 15574-15580.
Moon D S, Lee J K. Formation of wrinkled silica mesostructures based on the phase behavior of pseudoternary systems[J]. Langmuir, 2014, **30**(51): 15574-15580.[LinkOut]

[77] Qu Q, Li W, Wu Q. Formation Mechanism of Silica Particles with Dendritic Structure[J]. ChemistrySelect, 2019, **4**(21): 6656-6661.
Qu Q S, Li W Y, Wu Q. Formation mechanism of silica particles with dendritic structure[J]. ChemistrySelect, 2019, **4**(21): 6656-6661.[LinkOut]

[78] Dai Y, Yang D, Yu D, et al. Engineering of monodisperse core - shell up-conversion dendritic mesoporous silica nanocomposites with a tunable pore size[J]. Nanoscale, 2020, **12**(8): 5075-5083.
Dai Y, Yang D P, Yu D P, et al. Engineering of monodisperse core-shell up-conversion dendritic mesoporous silica nanocomposites with a tunable pore size[J]. Nanoscale, 2020, **12** (8): 5075-5083.[LinkOut]

[79] Shen D, Yang J, Li X, et al. Biphase stratification approach to three-dimensional dendritic biodegradable mesoporous silica nanospheres[J]. Nano Letters, 2014, **14**(2): 923-932.
Shen D K, Yang J P, Li X M, et al. Biphase stratification approach to three-dimensional dendritic biodegradable mesoporous silica nanospheres[J]. Nano Letters, 2014, **14**(2): 923-932.[PubMed]

[80] Firmansyah M L, Jalil A A, Triwahyono S, et al. Synthesis and Characterization of Fibrous Silica ZSM-5 for Cumene Hydrocracking[J]. Catalysis Science & Technology, 2016, **2016** (6): 5178-5182
Firmansyah M L, Jalil A A, Triwahyono S, et al. Synthesis and characterization of fibrous silica ZSM-5 for cumene hydrocracking [J]. Catalysis Science & Technology, 2016, **6**(13): 5178-5182.[LinkOut]

[81] Abdul Jalil A, Zolkifli A S, Triwahyono S, et al. Altering Dendrimer Structure of Fibrous-Silica-HZSM5 for Enhanced Product Selectivity of Benzene Methylation[J]. Industrial & Engineering Chemistry Research, 2019, **58**(2): 553-562.
Abdul Jalil A, Zolkifli A S, Triwahyono S, et al. Altering dendrimer structure of fibrous-silica-HZSM5 for enhanced product selectivity of benzene methylation[J]. Industrial & Engineering Chemistry Research, 2019, **58**(2): 553-562.[LinkOut]

[82] Rahman A F A, Jalil A A, Siang T J, et al. Mechanistic insight into low temperature toluene production via benzene methylation over mesopore-rich fibrous silica HZSM-5 zeolite[J]. Journal of Porous Materials, 2021, **28**(6): 1765-1777.
Rahman A F A, Jalil A A, Siang T J, et al. Mechanistic insight into low temperature toluene production *via* benzene methylation

over mesopore-rich fibrous silica HZSM-5 zeolite[J]. Journal of Porous Materials, 2021, **28**(6): 1765-1777.[LinkOut]

[83] Hussain I, Jalil A A, Mamat C R, et al. New insights on the effect of the H_2/CO ratio for enhancement of CO methanation over metal-free fibrous silica ZSM-5: Thermodynamic and mechanistic studies[J]. Energy Conversion and Management, 2019, **199**: 112056.
Hussain I, Jalil A A, Mamat C R, et al. New insights on the effect of the H_2/CO ratio for enhancement of CO methanation over metal-free fibrous silica ZSM-5: thermodynamic and mechanistic studies [J]. Energy Conversion and Management, 2019, **199**: 112056. [LinkOut]

[84] Teh L P, Triwahyono S, Jalil A A, et al. Fibrous silica mesoporous ZSM-5 for carbon monoxide methanation[J]. Applied Catalysis A General, 2016, **523**: 200-208.
Teh L P, Triwahyono S, Jalil A A, et al. Fibrous silica mesoporous ZSM-5 for carbon monoxide methanation[J]. Applied Catalysis A: General, 2016, **523**: 200-208.[LinkOut]

[85] Aziz F F A, Jalil A A, Triwahyono S, et al. Controllable structure of fibrous SiO_2 - ZSM-5 support decorated with TiO_2 catalysts for enhanced photodegradation of paracetamol[J]. Applied Surface Science, 2018, **455**: 84-95.
Aziz F F A, Jalil A A, Triwahyono S, et al. Controllable structure of fibrous SiO_2-ZSM-5 support decorated with TiO_2 catalysts for enhanced photodegradation of paracetamol[J]. Applied Surface Science, 2018, **455**: 84-95.[LinkOut]

[86] Hambali H U, Jalil A A, Abdulrasheed A A, et al. Fibrous spherical Ni-M/ZSM-5 (M: Mg, Ca, Ta, Ga) catalysts for methane dry reforming: The interplay between surface acidity-basicity and coking resistance[J]. International Journal of Energy Research, 2020, **44**(7): 5696-5712.
Hambali H U, Jalil A A, Abdulrasheed A A, et al. Fibrous spherical Ni-M/ZSM-5 (M: Mg, Ca, Ta, Ga) catalysts for methane dry reforming: the interplay between surface acidity-basicity and coking resistance[J]. International Journal of Energy Research, 2020, **44**(7): 5696-5712.[LinkOut]

[87] Hussain I, Jalil A A, Fatah N A A, et al. A highly competitive system for CO methanation over an active metal-free fibrous silica mordenite via in-situ ESR and FTIR studies[J]. Energy Conversion and Management, 2020, **211**: 112754.
Hussain I, Jalil A A, Fatah N A A, et al. A highly competitive system for CO methanation over an active metal-free fibrous silica mordenite *via in-situ* ESR and FTIR studies[J]. Energy Conversion and Management, 2020, **211**: 112754.[LinkOut]

[88] Hussain I, Jalil A A, Hassan N S, et al. Fabrication and characterization of highly active fibrous silica-mordenite ($FS@SiO_2$-MOR) cockscomb shaped catalyst for enhanced CO_2 methanation[J]. Chemical Engineering Science, 2020, **228**: 115978.
Hussain I, Jalil A A, Hassan N S, et al. Fabrication and characterization of highly active fibrous silica-mordenite ($FS@SiO_2$-MOR) cockscomb shaped catalyst for enhanced CO_2 methanation[J]. Chemical Engineering Science, 2020, **228**: 115978.[LinkOut]

[89] Izan S M, Triwahyono S, Jalil A A, et al. Additional Lewis acid sites of protonated fibrous silica@BEA zeolite (HSi@BEA) improving the generation of protonic acid sites in the isomerization of C6 alkane and cycloalkanes[J]. Applied Catalysis A: General, 2019, **570**: 228-237.
Izan S M, Triwahyono S, Jalil A A, et al. Additional Lewis acid sites of protonated fibrous silica@BEA zeolite (HSi@BEA) improving the generation of protonic acid sites in the isomerization of C_6 alkane and cycloalkanes[J]. Applied Catalysis A: General, 2019, **570**: 228-237.[LinkOut]

[90] Ghani N N M, Jalil A A, Triwahyono S, et al. Tailored mesoporosity and acidity of shape-selective fibrous silica beta zeolite for enhanced toluene co-reaction with methanol[J]. Chemical Engineering Science, 2019, **193**: 217-229.
Ghani N N M, Jalil A A, Triwahyono S, et al. Tailored mesoporosity and acidity of shape-selective fibrous silica beta zeolite for enhanced toluene co-reaction with methanol[J]. Chemical Engineering Science, 2019, **193**: 217-229.[LinkOut]

[91] Hussain I, Jalil A A, Hamid M Y S, et al. Substituted natural gas (SNG) production using an environment-friendly, metal-free modified beta zeolite (@BEA) catalyst with a dandelion flower-like structure[J]. Molecular Catalysis, 2022, **523**: 112140.
Hussain I, Jalil A A, Hamid M, et al. Substituted natural gas (SNG) production using an environment-friendly, metal-free modified beta zeolite (@BEA) catalyst with a dandelion flower-like structure[J]. Molecular Catalysis, 2022, **523**: 112140. [LinkOut]

[92] Jalil A A, Gambo Y, Ibrahim M, et al. Platinum-promoted fibrous silica Y zeolite with enhanced mass transfer as a highly selective catalyst for n-dodecane hydroisomerization[J]. International Journal of Energy Research, 2019, **0** (0): 1-16.
Jalil A A, Gambo Y, Ibrahim M, et al. Platinum-promoted fibrous silica Y zeolite with enhanced mass transfer as a highly selective catalyst for n-dodecane hydroisomerization[J]. International Journal of Energy Research, 2019, **43**(9): 4201-4216.[LinkOut]

[93] Triwahyono S, Jalil A A, Izan S M, et al. Isomerization of linear C5 - C7 over pt loaded on protonated fibrous silica@Y zeolite (Pt/HSi@Y) [J]. Journal of Energy Chemistry, 2019, **37**: 163-171.
Triwahyono S, Jalil A A, Izan S M, et al. Isomerization of linear C_5-C_7 over Pt loaded on protonated fibrous silica@Y zeolite (Pt/HSi@Y) [J]. Journal of Energy Chemistry, 2019, **37**: 163-171. [LinkOut]

[94] Chong C C, Bukhari S N, Cheng Y W, et al. Facile synthesis of tunable dendritic fibrous SBA-15 (DFSBA-15) with radial wrinkle structure[J]. Microporous and Mesoporous Materials, 2020, **294**: 109872.
Chong C C, Bukhari S N, Cheng Y W, et al. Facile synthesis of tunable dendritic fibrous SBA-15 (DFSBA-15) with radial wrinkle structure[J]. Microporous and Mesoporous Materials, 2020, **294**: 109872.[LinkOut]

[95] Chong C C, Setiabudi H D, Jalil A A. Dendritic fibrous SBA-15 supported nickel (Ni/DFSBA-15): A sustainable catalyst for hydrogen production[J]. International Journal of Hydrogen Energy, 2020, **45**(36): 18533-18548.
Chong C C, Setiabudi H D, Jalil A A. Dendritic fibrous SBA-15 supported nickel (Ni/DFSBA-15): a sustainable catalyst for hydrogen production[J]. International Journal of Hydrogen Energy, 2020, **45**(36): 18533-18548.[LinkOut]

[96] Chong C C, Cheng Y W, Setiabudi H D, et al. Dry reforming of methane over Ni/dendritic fibrous SBA-15 (Ni/DFSBA-15):

Optimization, mechanism, and regeneration studies[J]. International Journal of Hydrogen Energy, 2020, **45** (15): 8507-8525.

Chong C C, Cheng Y W, Setiabudi H D, et al. Dry reforming of methane over Ni/dendritic fibrous SBA-15 (Ni/DFSBA-15): optimization, mechanism, and regeneration studies[J]. International Journal of Hydrogen Energy, 2020, **45**(15): 8507-8525.[LinkOut]

[97] Abubakar Abdulkadir B, Mohd Zaki R S R, Abd Jalil A, et al. Synergistic effects of Fe_2O_3 supported on dendritic fibrous SBA-15 for superior photocatalytic degradation of methylene blue[J]. Materials Science in Semiconductor Processing, 2025, **185**: 108859.

Abubakar Abdulkadir B, Mohd Zaki R S R, Abd Jalil A, et al. Synergistic effects of Fe_2O_3 supported on dendritic fibrous SBA-15 for superior photocatalytic degradation of methylene blue[J]. Materials Science in Semiconductor Processing, 2025, **185**: 108859.[LinkOut]

[98] Hung C T, Duan L, Zhao T, et al. Gradient Hierarchically Porous Structure for Rapid Capillary-Assisted Catalysis[J]. Journal of the American Chemical Society, 2022, **144**(13): 6091-6099.

Hung C T, Duan L L, Zhao T C, et al. Gradient hierarchically porous structure for rapid capillary-assisted catalysis[J]. Journal of the American Chemical Society, 2022, **144**(13): 6091-6099.[PubMed]

[99] Peng H, Xu L, Wu H, et al. One-pot synthesis of benzamide over a robust tandem catalyst based on center radially fibrous silica encapsulated TS-1[J]. Chemical Communications, 2013, **49**(26): 2709-2711.

Peng H G, Xu L, Wu H H, et al. One-pot synthesis of benzamide over a robust tandem catalyst based on center radially fibrous silica encapsulated TS-1[J]. Chemical Communications, 2013, **49** (26): 2709-2711.[LinkOut]

[100] Peng H, Wang D, Xu L, et al. One-pot synthesis of primary amides on bifunctional Rh(OH)x/TS-1@KCC-1 catalysts[J]. Chinese Journal of Catalysis, 2013, **34**(11): 2057 - 2065.

Peng H G, Wang D R, Xu L, et al. One-pot synthesis of primary amides on bifunctional $Rh(OH)_x$/TS-1@KCC-1 catalysts[J]. Chinese Journal of Catalysis, 2013, **34**(11): 2057-2065.[LinkOut]

[101] Mosaad Awad M, Hussain I, Ahmed Taialla O, et al. Unveiling the catalytic performance of unique core-fibrous shell silica-lanthanum oxide with different nickel loadings for dry reforming of methane[J]. Energy Conversion and Management, 2024, **311**: 118508.

Mosaad Awad M, Hussain I, Ahmed Taialla O, et al. Unveiling the catalytic performance of unique core-fibrous shell silica-lanthanum oxide with different nickel loadings for dry reforming of methane[J]. Energy Conversion and Management, 2024, **311**: 118508.[LinkOut]

[102] Shabir J, Rani S, Sharma M, et al. Synthesis of dendritic fibrous nanosilica over a cubic core ($cSiO_2$@DFNS) with catalytically efficient silver nanoparticles for reduction of nitroarenes and degradation of organic dyes[J]. RSC Advances, 2020, **10**(14): 8140-8151.

Shabir J, Rani S, Sharma M, et al. Synthesis of dendritic fibrous nanosilica over a cubic core ($cSiO_2$@DFNS) with catalytically efficient silver nanoparticles for reduction of nitroarenes and degradation of organic dyes[J]. RSC Advances, 2020, **10**(14): 8140-8151.[LinkOut]

[103] Qu Q, Min Y, Zhang L, et al. Silica Microspheres with Fibrous Shells: Synthesis and Application in HPLC[J]. Analytical Chemistry, 2015, **87**(19): 9631-9638.

Qu Q S, Min Y, Zhang L H, et al. Silica microspheres with fibrous shells: synthesis and application in HPLC[J]. Analytical Chemistry, 2015, **87**(19): 9631-9638.[LinkOut]

[104] Qu Q, Si Y, Xuan H, et al. Synthesis of core-shell silica spheres with tunable pore diameters for HPLC[J]. Materials Letters, 2018, **211**: 40-42.

Qu Q S, Si Y, Xuan H, et al. Synthesis of core-shell silica spheres with tunable pore diameters for HPLC[J]. Materials Letters, 2018, **211**: 40-42.[LinkOut]

[105] Qu Q, Si Y, Xuan H, et al. Dendritic core-shell silica spheres with large pore size for separation of biomolecules[J]. Journal of Chromatography A, 2018, **1540**: 31-37.

Qu Q S, Si Y, Xuan H, et al. Dendritic core-shell silica spheres with large pore size for separation of biomolecules[J]. Journal of Chromatography A, 2018, **1540**: 31-37.[LinkOut]

[106] Qu Q, Xuan H, Zhang K, et al. Core-shell silica particles with dendritic pore channels impregnated with zeolite imidazolate framework-8 for high performance liquid chromatography separation[J]. Journal of Chromatography A, 2017, **1505**: 63-68.

Qu Q S, Xuan H, Zhang K H, et al. Core-shell silica particles with dendritic pore channels impregnated with zeolite imidazolate framework-8 for high performance liquid chromatography separation[J]. Journal of Chromatography A, 2017, **1505**: 63-68.[LinkOut]

[107] Irfan A, Feng W, Liu K, et al. TiO_2-modified fibrous core-shell mesoporous material to selectively enrich endogenous phosphopeptides with proteins exclusion prior to CE-MS analysis [J]. Talanta, 2021, **235**: 122737.

Irfan A, Feng W X, Liu K X, et al. TiO_2-modified fibrous core-shell mesoporous material to selectively enrich endogenous phosphopeptides with proteins exclusion prior to CE-MS analysis [J]. Talanta, 2021, **235**: 122737.[LinkOut]

[108] Liu J, Feng W, Tian M, et al. Titanium dioxide-coated core-shell silica microspheres-based solid-phase extraction combined with sheathless capillary electrophoresis-mass spectrometry for analysis of glyphosate, glufosinate and their metabolites in baby foods[J]. Journal of Chromatography A, 2021, **1659**: 462519.

Liu J N, Feng W X, Tian M M, et al. Titanium dioxide-coated core-shell silica microspheres-based solid-phase extraction combined with sheathless capillary electrophoresis-mass spectrometry for analysis of glyphosate, glufosinate and their metabolites in baby foods[J]. Journal of Chromatography A, 2021, **1659**: 462519.[LinkOut]

[109] Wang A, Hu L, Liu J, et al. Polyaniline-coated core-shell silica microspheres-based dispersive-solid phase extraction for detection of benzophenone-type UV filters in environmental water samples[J]. Environmental Advances, 2021, **3**: 100037.

Wang A P, Hu L H, Liu J N, et al. Polyaniline-coated core-shell silica microspheres-based dispersive-solid phase extraction for detection of benzophenone-type UV filters in environmental water samples[J]. Environmental Advances, 2021, **3**: 100037.[LinkOut]

[110] Zhang W, Li S M, Zhang J. Preparation and Chromatographic

Features of Fibrous Core – Shell HPLC Packing Material[J]. Chromatographia, 2018, **81**(9): 1249–1256.
Zhang W, Li S M, Zhang J. Preparation and chromatographic features of fibrous core-shell HPLC packing material[J]. Chromatographia, 2018, **81**(9): 1249–1256.[LinkOut]

[111] Siddiki A K M N A, Lin J, Balkus K J. Encapsulation of ZnO and Ho:ZnO Nanoparticles in the Core of Wrinkled Mesoporous Silica [J]. Langmuir, 2023, **39**(36): 12956–12965.
Siddiki A K M N A, Lin J, Balkus K J. Encapsulation of ZnO and Ho: ZnO nanoparticles in the core of wrinkled mesoporous silica [J]. Langmuir, 2023, **39**(36): 12956–12965.[LinkOut]

[112] Wang C, Guo T, Tang R, et al. Facile Fabrication of Monodisperse Vinyl Hybrid Core – Shell Silica Microsphere with Short Range Radial Channel in bi-phase System[J]. Small, 2025, **21**(8): 2409640.
Wang C Y, Guo T T, Tang R Z, et al. Facile fabrication of monodisperse vinyl hybrid core-shell silica microsphere with short range radial channel in bi-phase system[J]. Small, 2025, **21**(8): 2409640.[LinkOut]

[113] Sun J, Zhang P, Yan K, et al. High-performance nanothermometry system with controlled sensitivity based on dual-emission $CsPbBr_3$/CdTe@SiO_2 core/shell nanocomposites[J]. Journal of Colloid and Interface Science, 2025, **693**: 137607.
Sun J N, Zhang P, Yan K, et al. High-performance nanothermometry system with controlled sensitivity based on dual-emission $CsPbBr_3$/CdTe@SiO_2 core/shell nanocomposites[J]. Journal of Colloid and Interface Science, 2025, **693**: 137607.[LinkOut]

[114] Liu S, Li W, Dong S, et al. An all-in-one theranostic nanoplatform based on upconversion dendritic mesoporous silica nanocomposites for synergistic chemodynamic/photodynamic/gas therapy[J]. Nanoscale, 2020, **12**(47): 24146–24161.
Liu S K, Li W T, Dong S M, et al. An all-in-one theranostic nanoplatform based on upconversion dendritic mesoporous silica nanocomposites for synergistic chemodynamic/photodynamic/gas therapy[J]. Nanoscale, 2020, **12**(47): 24146–24161.[LinkOut]

[115] Dong Y, Dong S, Wang Z, et al. Multimode Imaging-Guided Photothermal/Chemodynamic Synergistic Therapy Nanoagent with a Tumor Microenvironment Responded Effect[J]. ACS Applied Materials & Interfaces, 2020, **12**(47): 52479–52491.
Dong Y S, Dong S M, Wang Z, et al. Multimode imaging-guided photothermal/chemodynamic synergistic therapy nanoagent with a tumor microenvironment responded effect[J]. ACS Applied Materials & Interfaces, 2020, **12**(47): 52479–52491.[PubMed]

[116] Xu Y, Liang H, Zeng Q, et al. A bubble-enhanced lanthanide-doped up/down-conversion platform with tumor microenvironment response for dual-modal photoacoustic and near-infrared-II fluorescence imaging[J]. Journal of Colloid and Interface Science, 2024, **659**: 149–159.
Xu Y N, Liang H R, Zeng Q T, et al. A bubble-enhanced lanthanide-doped up/down-conversion platform with tumor microenvironment response for dual-modal photoacoustic and near-infrared-II fluorescence imaging[J]. Journal of Colloid and Interface Science, 2024, **659**: 149–159.[LinkOut]

[117] Dong S, Dong Y, Jia T, et al. GSH-Depleted Nanozymes with Hyperthermia-Enhanced Dual Enzyme-Mimic Activities for Tumor Nanocatalytic Therapy[J]. Advanced Materials, 2020, **32**(42): 2002439.
Dong S M, Dong Y S, Jia T, et al. GSH-depleted nanozymes with hyperthermia-enhanced dual enzyme-mimic activities for tumor nanocatalytic therapy[J]. Advanced Materials, 2020, **32**(42): e2002439.[PubMed]

[118] Abbaraju P L, Yang Y, Yu M, et al. Core – Shell - structured Dendritic Mesoporous Silica Nanoparticles for Combined Photodynamic Therapy and Antibody Delivery[J]. Chemistry – An Asian Journal, 2017, **12**(13): 1465–1469.
Abbaraju P L, Yang Y N, Yu M H, et al. Core-shell-structured dendritic mesoporous silica nanoparticles for combined photodynamic therapy and antibody delivery[J]. Chemistry-An Asian Journal, 2017, **12**(13): 1465–1469.[LinkOut]

[119] Wan M M, Wang Q, Wang R L, et al. Platelet-derived porous nanomotor for thrombus therapy[J]. Science Advances, 2020, **6**(22): eaaz9014.
Wan M M, Wang Q, Wang R L, et al. Platelet-derived porous nanomotor for thrombus therapy[J]. Science Advances, 2020, **6**(22): eaaz9014.[PubMed]

[120] Wan M, Wang Q, Li X, et al. Systematic Research and Evaluation Models of Nanomotors for Cancer Combined Therapy[J]. Angewandte Chemie International Edition, 2020, **59**: 14458.
Wan M M, Wang Q, Li X Y, et al. Systematic research and evaluation models of nanomotors for cancer combined therapy[J]. Angewandte Chemie International Edition, 2020, **59**(34): 14458–14465.[LinkOut]

[121] Liu S, Zhao Y, Shen M, et al. Hyaluronic acid targeted and pH-responsive multifunctional nanoparticles for chemo-photothermal synergistic therapy of atherosclerosis[J]. Journal of Materials Chemistry B, 2021, **10**: 562.
Liu S, Zhao Y, Shen M L, et al. Hyaluronic acid targeted and pH-responsive multifunctional nanoparticles for chemo-photothermal synergistic therapy of atherosclerosis[J]. Journal of Materials Chemistry B, 2022, **10**(4): 562–570.[LinkOut]

[122] Xu C, Chen F, Valdovinos H F, et al. Bacteria-like mesoporous silica-coated gold nanorods for positron emission tomography and photoacoustic imaging-guided chemo-photothermal combined therapy[J]. Biomaterials, 2018, **165**: 56–65.
Xu C, Chen F, Valdovinos H F, et al. Bacteria-like mesoporous silica-coated gold nanorods for positron emission tomography and photoacoustic imaging-guided chemo-photothermal combined therapy[J]. Biomaterials, 2018, **165**: 56–65.[LinkOut]

[123] Wang Z, Fu X, Dai C, et al. NIR II-triggered core-shell upconversion nanocomposites for peroxynitrite-boosted anti-infection against diabetic wound[J]. Chemical Engineering Journal, 2024, **480**: 148271.
Wang Z K, Fu X Y, Dai C X, et al. NIR II-triggered core-shell upconversion nanocomposites for peroxynitrite-boosted anti-infection against diabetic wound[J]. Chemical Engineering Journal, 2024, **480**: 148271.[LinkOut]

[124] Kashfi-Sadabad R, Gonzalez-Fajardo L, Hargrove D, et al. Engineering Multifunctional Gold Decorated Dendritic Mesoporous Silica/Tantalum Oxide Nanoparticles for Intraperitoneal Tumor-Specific Delivery[J]. Particle & Particle Systems Characterization, 2019, **36**(4): 1900058.
Kashfi-Sadabad R, Gonzalez-Fajardo L, Hargrove D, et al. Engineering multifunctional gold decorated dendritic mesoporous

silica/tantalum oxide nanoparticles for intraperitoneal tumor-specific delivery[J]. Particle & Particle Systems Characterization, 2019, **36**(4): 1900058.[LinkOut]

[125] Li Z, Lu S, Liu W, et al. Synergistic lysozyme-photodynamic therapy against resistant bacteria based on an intelligent upconversion nanoplatform[J]. Angewandte Chemie International Edition, 2021, **60**(35): 19201-19206.
Li Z, Lu S, Liu W Z, et al. Synergistic lysozyme-photodynamic therapy against resistant bacteria based on an intelligent upconversion nanoplatform[J]. Angewandte Chemie International Edition, 2021, **60**(35): 19201-19206.[LinkOut]

[126] Chen Y, Zuo C, Ma X, et al. Solid-silica core/mesoporous-silica shell composite abrasives: synthesis, characterization, and the effect of mesoporous shell structures on CMP[J]. Journal of Materials Science: Materials in Electronics, 2018, **29**(5): 3817-3828.
Chen Y, Zuo C Z, Ma X Y, et al. Solid-silica core/mesoporous-silica shell composite abrasives: synthesis, characterization, and the effect of mesoporous shell structures on CMP[J]. Journal of Materials Science: Materials in Electronics, 2018, **29**(5): 3817-3828.[LinkOut]

[127] Chen A, Mu H, Zuo C, et al. Fabrication, characterization, and CMP performance of dendritic mesoporous-silica composite particles with tunable pore sizes[J]. Journal of Alloys and Compounds, 2019, **770**: 335-344.
Chen A L, Mu H L, Zuo C Z, et al. Fabrication, characterization, and CMP performance of dendritic mesoporous-silica composite particles with tunable pore sizes[J]. Journal of Alloys and Compounds, 2019, **770**: 335-344.[LinkOut]

[128] Chen A, Ma X, Cai W, et al. Polystyrene-supported dendritic mesoporous silica hybrid core/shell particles: controlled synthesis and their pore size-dependent polishing behavior[J]. Journal of Materials Science, 2020, **55**(2): 577-590.
Chen A L, Ma X Y, Cai W J, et al. Polystyrene-supported dendritic mesoporous silica hybrid core/shell particles: controlled synthesis and their pore size-dependent polishing behavior[J]. Journal of Materials Science, 2020, **55**(2): 577-590.[LinkOut]

[129] Wang Y, He J, Shi Y, et al. Structure-dependent adsorptive or photocatalytic performances of solid and hollow dendritic mesoporous silica&titania nanospheres[J]. Microporous and Mesoporous Materials, 2020, **305**: 110326.
Wang Y B, He J, Shi Y M, et al. Structure-dependent adsorptive or photocatalytic performances of solid and hollow dendritic mesoporous silica & titania nanospheres[J]. Microporous and Mesoporous Materials, 2020, **305**: 110326.[LinkOut]

[130] Yu H, Zhang Q, Dahl M, et al. Dual-pore Carbon Shells for Efficient Removal of Humic Acid from Water[J]. Chemistry - A European Journal, 2017, **23**: 16249-16256.
Yu H X, Zhang Q, Dahl M, et al. Dual-pore carbon shells for efficient removal of humic acid from water[J]. Chemistry-A European Journal, 2017, **23**(64): 16249-16256.[LinkOut]

[131] Jingru Z, Hongtao C, Jiaqi C, et al. Preparation and application of KCC-1@ZIF-8 for the solid extraction of tetracycline with high adsorption capacity[J]. Analytical Methods, 2024, **16**(35): 5959-5970.
Zhang J R, Chu H T, Chen J Q, et al. Preparation and application of KCC-1@ZIF-8 for the solid extraction of tetracycline with high adsorption capacity[J]. Analytical Methods, 2024, **16**(35): 5959-5970.[PubMed]

[132] Tran N M, Jung S, Yoo H. "Nanospace engineering" by the growth of nano metal-organic framework on dendritic fibrous nanosilica (DFNS) and DFNS/gold hybrids[J]. Nano Research, 2020, **13**(3): 775-784.
Tran N M, Jung S, Yoo H. "Nanospace engineering" by the growth of nano metal-organic framework on dendritic fibrous nanosilica (DFNS) and DFNS/gold hybrids[J]. Nano Research, 2020, **13**(3): 775-784.[LinkOut]

[133] Zhang S, Wen L, Yang J, et al. Facile Fabrication of Dendritic Mesoporous SiO_2@CdTe@SiO_2 Fluorescent Nanoparticles for Bioimaging[J]. Particle and Particle Systems Characterization, 2016, **33**(5): 261 - 270.
Zhang S H, Wen L, Yang J P, et al. Facile fabrication of dendritic mesoporous SiO_2@CdTe@SiO_2 fluorescent nanoparticles for bioimaging[J]. Particle & Particle Systems Characterization, 2016, **33**(5): 261-270.[LinkOut]

[134] Huang L, Liao T, Wang J, et al. Brilliant Pitaya-Type Silica Colloids with Central - Radial and High-Density Quantum Dots Incorporation for Ultrasensitive Fluorescence Immunoassays[J]. Advanced Functional Materials, 2018, **28**(4): 1705380.
Huang L, Liao T, Wang J, et al. Brilliant pitaya-type silica colloids with central-radial and high-density quantum dots incorporation for ultrasensitive fluorescence immunoassays[J]. Advanced Functional Materials, 2018, **28**(4): 1705380.[LinkOut]

[135] Leng Y, Wang X, Li W, et al. Enabling ultrahigh loading of AIEgens through alkyne-amine click reactions for highly sensitive colorimetric-fluorescent dual-readout lateral flow immunoassay [J]. Sensors and Actuators B: Chemical, 2025, **432**: 137473.
Leng Y K, Wang X L, Li W J, et al. Enabling ultrahigh loading of AIEgens through alkyne-amine click reactions for highly sensitive colorimetric-fluorescent dual-readout lateral flow immunoassay [J]. Sensors and Actuators B: Chemical, 2025, **432**: 137473.[LinkOut]

[136] Wu Q, Huang F, Jiang Y, et al. Firefly lantern-inspired AIE-enhanced gold nanocluster microspheres for ultrasensitive detection of foodborne pathogenic bacteria[J]. Sensors and Actuators B: Chemical, 2025, **422**: 136584.
Wu Q L, Huang F Y, Jiang Y Y, et al. Firefly lantern-inspired AIE-enhanced gold nanocluster microspheres for ultrasensitive detection of foodborne pathogenic bacteria[J]. Sensors and Actuators B: Chemical, 2025, **422**: 136584.[LinkOut]

[137] Wang Y, Tao J, Wang Y, et al. Remarkable reduction ability towards p-nitrophenol by a synergistic effect against the aggregation and leaching of palladium nanoparticles in dendritic supported catalysts[J]. Applied Surface Science, 2022, **574**: 151702.
Wang Y B, Tao J H, Wang Y N, et al. Remarkable reduction ability towards *p*-nitrophenol by a synergistic effect against the aggregation and leaching of palladium nanoparticles in dendritic supported catalysts[J]. Applied Surface Science, 2022, **574**: 151702.[LinkOut]

[138] Wang Y, He J, Li X, et al. Dendritic mesoporous silica&titania nanospheres (DMSTNs) coupled with amorphous carbon nitride (ACN) for improved visible-light-driven hydrogen production[J]. Applied Surface Science, 2021, **538**: 148147.

Wang Y B, He J, Li X L, et al. Dendritic mesoporous silica&titania nanospheres (DMSTNs) coupled with amorphous carbon nitride (ACN) for improved visible-light-driven hydrogen production[J]. Applied Surface Science, 2021, **538**: 148147. [LinkOut]

[139] Azizi S, Shadjou N, Soleymani J. CuI/Fe_3O_4 NPs@Biimidazole IL-KCC-1 as a leach proof nanocatalyst for the synthesis of imidazo [1, 2-a]pyridines in aqueous medium[J]. Applied Organometallic Chemistry, 2021, **35**(1): e6031.

Azizi S, Shadjou N, Soleymani J. CuI/Fe_3O_4 NPs@Biimidazole IL-KCC-1 as a leach proof nanocatalyst for the synthesis of imidazo [1, 2-α] pyridines in aqueous medium[J]. Applied Organometallic Chemistry, 2021, **35**(1): e6031.[LinkOut]

[140] Yang Y, Lu Y, Abbaraju P L, et al. Multi-shelled dendritic mesoporous organosilica hollow spheres: Roles of composition and architecture in cancer immunotherapy[J]. Angewandte Chemie International Edition, 2017, **56**(29): 8446-8450.

Yang Y N, Lu Y, Abbaraju P L, et al. Multi-shelled dendritic mesoporous organosilica hollow spheres: roles of composition and architecture in cancer immunotherapy[J]. Angewandte Chemie International Edition, 2017, **56**(29): 8446-8450.[LinkOut]

[141] Munaweera I, Trinh M, Hong J, et al. Chemically powered nanomotor as a delivery vehicle for biologically relevant payloads [J]. Journal of Nanoscience and Nanotechnology, 2016, **16**(9): 9063-9071.

Munaweera I, Trinh M, Hong J, et al. Chemically powered nanomotor as a delivery vehicle for biologically relevant payloads [J]. Journal of Nanoscience and Nanotechnology, 2016, **16**(9): 9063-9071.[LinkOut]